Title:	Reinterpretation of Mariner 9 IRIS Data on the Basis of a Simulation of Radiative-Conductive-Convective Transfer in the Dust-laden Martian Atmosphere.
Report Date:	November 1974
Author:	A. J. Pallmann
Performing Organization Report No.:	PLATMOS Rept #9
Performing Organization Name and Address:	Saint Louis University 221 N. Grand Saint Louis, Missouri 63103
Grant No.:	NGR 26-006-042
Sponsoring Agency Name and Address:	National Aeronautics and Space Administration Washington, D.C. 20546
Type of Report:	Contractor Report (Final) covering the Period October 1973 - December 1974

Supplementary Notes:

This report presents further findings developed in continuation of a several-years research effort sponsored by NASA. See Contractor Report CR-2318.

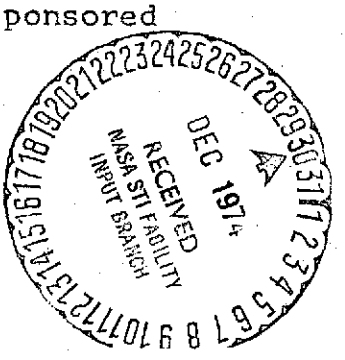

SAINT LOUIS UNIVERSITY

DEPARTMENT OF EARTH AND ATMOSPHERIC SCIENCES

3507 LACLEDE AVENUE
SAINT LOUIS, MISSOURI 63103

MAILING ADDRESS:
P. O. BOX 8099 - LACLEDE STATION
SAINT LOUIS, MISSOURI 63156

December 27, 1974

NASA Scientific and Technical Information
Facility
P.O. Box 33
College Park, Maryland 20740

Gentlemen:

Enclosed please find two copies of the final report on the NASA sponsored research project under Grant NGR 26-006-042.

Sincerely,

Albert Pallmann

Albert J. Pallmann
Principal Investigator
Grant No. NGR 26-006-042

AJP/fb

Enc.

Abstract

Time-dependent vertical distributions of atmospheric temperature and static stability were determined by a radiative-convective-conductive heat transfer model attuned to Mariner 9 IRIS radiance data. Of particular interest were conditions of both the dust-laden and dust-free atmosphere in the middle latitudes on Mars during the late S.H. summer season.

The numerical model simulates at high spatial and temporal resolution (52 atmospheric and 30 subsurface levels; with a time-step of 7.5 min.) the heat transports in the ground-atmosphere system. The algorithm is based on the solution of the appropriate heating rate equation which includes radiative, molecular-conductive and convective heat transfer terms. Ground and atmosphere are coupled by an internal thermal boundary condition.

The attunement of the model to the measured IRIS radiance data was achieved by modulating the temperature sounding input until the running mean square of the relative difference between the measured and simulated values was less than .04 (window 200 cm^{-1}). Refined spectroscopic data for CO_2 absorption improved the quantitative representation of the interaction between the gaseous constituent and the radiative quanta in transfer. A multiphase simulation of the impact of dust on the thermal structure was undertaken.

It was found that high spatial- and temporal-resolution temperature soundings, generated by the attuned model, serve to adjust the IRIS inverted temperature data in the presence of dust.

Key Words (Suggested by Author)

-Martian Atmosphere
-Dust-laden Atmosphere
-Radiative-Convective Heat Transfer
-Ground-Atmosphere Interface Energetics
-Simulation attuned to Satellite Data

LIST OF FIGURES AND TABLE

TABLE OF CONTENTS

FOREWORD AND ACKNOWLEDGEMENTS

This is the final report of a fourteen-months' project sponsored by the Planetary Atmospheres Program, Office of Space Science, NASA Headquarters, under grant No. NGR 26-006-042. The author is indebted to Dr. Robert F. Fellows, Chief of Planetary Atmospheres, NASA Planetary Programs, who served as the technical officer for this grant.

By incorporating a convective heat transport subroutine into the existing model of radiative-conductive transfer of thermal energy within the soil and dust-laden atmospheric subsystems, an investigative tool of simulation became available to be attuned to the measured IRIS signals of Mariner 9. The "AFCRL Atmospheric Absorption Line Parameters Compilation" afforded this project improved spectroscopic data for carbon dioxide. More than 9,000 individual CO_2 absorption lines were taken up by a particular quasi-random transmission function.

The radiative-conductive-convective heat transfer model, attuned to IRIS output signals, generated temperature soundings which were successfully utilized to reinterpret inverted IRIS soundings. The author wishes to express his gratitude to Drs. R. A. Hanel and J. C. Pearl of Goddard Space Flight Center for generously releasing Mariner 9 IRIS data, to Dr. R. A. McClatchey of AFCRL Optical Physics Laboratories for making a whole tape of absorption line data available, and to Dr. John Shaw of Ohio State University for fruitful discussion. Special thanks are due to Mr. Eric Bram who carried out the tedious task of scientific computing with dedication and talent.

1.0 INTRODUCTION; OBJECTIVES OF REPORT

A global-scale dust storm in the Martian atmosphere during the first phase of the Mariner 9 orbital mission precluded a direct application of the particular integral inversion technique developed for the IRIS experiment (Hanel et alii, 1972). The extent of the impact of the opaque dust layer on the IRIS radiance spectra and on the resultant distortions of the inverted data is not yet fully understood. Especially the thermal stratification of the lowest 6 km is open to further investigation.

Existing IRIS measurements directly lend themselves to additional analysis which utilizes a radiative-conductive-convective transfer model. This model includes a particular algorithm to account for the effects of dust on the temperature structure in the vertical. The basic details of the model are described in recent publications (Pallmann and Dannevik, 1972; Pallmann and Frisella, 1972; and Pallmann et alii, 1973).

The basic objective of this study is to submit the Mariner 9 IRIS radiance signals and inverted temperature soundings to a reinterpretation using the aforementioned computer model in a highly time-sensitive mode to simulate the impact of the opaque dust layer on the atmospheric temperature soundings. The reinterpretation is performed on a greatly enhanced data base provided by a computer model

which establishes a high resolution time-continuity between discrete IRIS measurements. The spatial resolving power is particularly fine in the lowest atmospheric layers providing 11 data points over the first 6 km of elevation.

A second objective is to gain further insight into the interaction between atmospheric polydispersions and radiative transfer processes which can then be applied to other atmospheric systems in which similar conditions occur, e.g., polluted urban boundary layer.

2.0 COMPUTATIONAL MODEL OF MARTIAN GROUND-ATMOSPHERE SYSTEM

2.1 DESCRIPTION OF MODEL

The details of a radiative-conductive heat transfer model have been described by Pallmann et alii (1973). Some of the basic characteristics of this model are that it assumes a pure carbon dioxide atmosphere of 50 km depth, in local thermodynamic equilibrium (LTE), and exhibits plane-parallel stratification. The impact of suspended dust particulates on gaseous absorption is taken into account. Doppler broadening is considered negligible as well as the effects of molecular scattering.

The lower solid surface of the model atmosphere is taken to be a flat, uniform sand-like material. The surface diffusely reflects solar radiation in accordance with a radiometric albedo, and emits as a gray body. The ground-atmosphere interface temperature and the thermal structure below the surface are determined as a function of time.

The governing relations are the appropriate heating rate equations for atmosphere and subsurface system, as presented in the aforementioned publication. The spectral radiative net flux for the case of LTE includes long-wave upward and downward flux integrals, ground emission and a solar flux integral. All of these terms

incorporate attenuation functions. The requirement of continuity of heat flux at the ground surface takes the form of a balance equation for all heat transports through long- and short-wave radiation, soil conduction, and atmospheric conduction. (For convection see Sec. 2.21.) The additional boundary and initial conditions are standard.

The numerical algorithm includes a quasi-random transmission function after Goody (1964). Particular provisions are made for weak- and strong-line absorption, and a heteorogeneous pressure and temperature stratification. For details on the finite difference form of the governing equations the reader is referred to the aforementioned paper.

2.2 EXPANSION OF MODEL

Former simulations by the radiative-conductive model clearly showed the presence of a steep superadiabatic stratification in the lowest atmospheric layers during the hours from mid-morning to early afternoon. Some of the results of this earlier simulation effort have been reported by Dannevik and Pallmann (1974).* Of particular interest is the development of a free-atmospheric convective layer at the top of the dust layer if the dust concentration between 30 and 40 km is still relatively high dropping off beyond this altitude.

* See Appendix.

It was concluded that a particular subroutine for convective heat transport had to be incorporated into the computer model. Furthermore, it appeared beneficial to overhaul the whole computer program with the objective of gaining a higher degree of efficiency.

2.21 INCLUSION OF CONVECTIVE HEAT TRANSFER

In order to model such convective overturns an additional subroutine for the program was developed. The principle of enthalpy conservation was adopted as the basis for convective heat transport.

The subroutine was written in such a way that the computer accepted the strictly radiative-conductive temperature distribution as a first guess. Whenever a superadiabatic stratification was found in a given layer the convective adjustment redistributed the enthalpy of the respective layer by establishing the adiabatic lapse rate. The governing relationship is the Poisson equation which relates temperature, pressure and potential temperature.

At the ground-atmosphere interface, heat is also convectively transferred into the "air" due to solar overheating of the sand surface. We followed a particular approach developed by Kraichnan (1959). He derived an explicit formula for the convective heat flux into the

surface boundary layer (constant flux layer). We have adapted this equation to the specific condition on Mars and arrived at the expression

$$(1)\quad F^* = \left[3.005287\ (TMARS - TCT1)\cdot \left(\frac{TMARS}{TCT1} - 1\right)^{1/3}\right] * RHO * CP$$

with

F*: convective heat flux off the ground.

TMARS: surface temperature at the beginning of primary step.

TCT1: temperature at 12.5 m at the beginning of primary step.

RHO: density at 12.5 m.

CP: specific heat a constant pressure of CO_2 (8.2×10^6 ergs $g^{-1}\ {}^{o}K^{-1}$).

If for a given computational time step TMARS turns out to be greater than (TCT1), the program will calculate the "pumping" of convective heat F* due to equation (1). It proceeds to determine a new temperature value at 12.5 m by applying a forward time step.

This particular procedure involves a searching technique starting from the top of the atmosphere downward. The computer is asked to find the first position (if there is one) for which the temperature lapse rate is greater than the adiabatic rate and correct for it by applying the enthalpy conservation principle. The corrective search

is continued downward to and including the level at the top of the constant flux layer.

Thus, for a given forward time step a final temperature profile results which is nowhere steeper than the adiabatic lapse rate. The same procedure is applicable to the time period for which convective overturn declines and ceases to exist. Frequently, this happens in the later afternoon.

2.22 IMPROVEMENT OF SPECTROSCOPIC RESPONSE OF MODEL

Under the conditions of low surface pressure and high CO_2 abundance, weak absorption bands are considerably enhanced (Drayson, 1972). This behavior is of special importance for remote sounding. Special care must be taken in the spectral regions containing Q-branches. In addition, the atmospheric temperatures on Mars are lower such that the temperature dependence of the Lorentz half-width becomes more important. For the intermediate IR, the integrated line intensity is dependent on temperature. Very low temperatures reduce the line intensity drastically. (See for example Pallmann, 1968).

These various aspects demonstrate the need for a refined spectral resolution in the calculation of the transmission function. Several researchers suggested spectral increments between 5 and 20 cm^{-1} depending on the particular wave-number range. An additional factor is given

by the kind of transmission function someone chooses to use. Our model incorporates a quasi-random transmittance. Thus, we assume that the lines are placed at random with respect to wave-number implying a Poisson distribution of the spacing between lines.

Therefore, we have chosen as increment of 5 cm^{-1} for the computation at 50 km of spectral and integrated upward flux within the spectral interval (200 - 2,000) cm^{-1}.

The refined increment of 5 cm^{-1} requires a compilation of atmospheric CO_2 absorption line parameters offering as many weak lines as possible and a better quality of the data. (Dr. J. Shaw of Ohio State University suggested that I acquire a magnetic tape copy of the AFCRL compilation of 1973).

3.0 REFINED ATMOSPHERIC ABSORPTION LINE PARAMETERS FOR CO_2

Several years ago, the Optical Physics Laboratory of AFCRL initiated a program of compiling spectroscopic data on individual vibration-rotation lines of various polyatomic molecules with significance in the atmosphere. This compilation was published in 1973 by McClatchey et alii. It includes data on more than 9,000 lines for CO_2. We obtained a copy of the data tape and extracted the CO_2 absorption line parameters such as integrated line intensity, Lorentz half-width, energy of the lower state, rotation and vibration identification, date and isotope against wave-number. The description of the compilation assisted us in adjusting some details of the computer model, which led to improved calculations of the transmission function (See Sect. 2.22). The model computations which generated spectral upward flux at the top of the atmosphere and, through the solution of the heating rate equation, temperature soundings, are considered a better quality product than was previously attainable.

4.0 ATTUNEMENT OF MODEL TO IRIS RADIANCE SIGNALS

4.1 BASIC ASPECTS RELATING TO ATTUNEMENT

In general terms, the method of data analysis will consist of correlating and examining for consistency the Mariner 9 IRIS smoothed radiance measurements, derived inverted temperature soundings and the spectral flux and temperature distribution outputs of the radiative-conductive-convective simulation model developed for both dust-laden and dust-free atmospheric conditions on Mars. The model simulates several of the essential physical mechanisms at work in the Martian lower atmosphere. The time evolution of these mechanisms requires a refined temporal resolution for the model output data in order to render a more realistic time-dependent fine-structure of the temperature stratification especially in the lowest 6 km.

Some evidence was presented by Pallmann and Frisella (1972) and Pallmann et alii (1973) that an inverted IRIS sounding of the S.H. polar region during late summer becomes drastically modified over a period of one to two days. This is interpreted to indicate that non-negligible distortions have been introduced into the inverted data by the presence of dust.

The length of the computational time step turns out to be very critical. After some optimization study, it was decided to take 7.5 minutes except for the period when convective overturn ceases in the afternoon. For this condition, the time step was reduced to 3 minutes.

The optimized time step assures a balanced diurnal cycle of the atmospheric response to the solar forcing cycle. If for a given instance, namely the moment the IRIS spectrometer generates a scan over a particular target area, the simulation becomes attuned to the smoothed IRIS signal function, the consistency carries over into the balanced cycle of time evolution.

In this context, some consideration must be given to the need for a refined spectroscopic take up within the model (sub-sect. 4.11), the largest possible width of the spectroscopic range (sub-sect. 4.12), and the interactions within the master-loop of the program performing the dual integration over the wave-number and depth ranges (sub-sect. 4.13). In the sub-sect. 4.14, some methodological advantage is discussed in providing for the outputs a distinction between the components of ground and atmospheric upward flux leaving the top of the atmosphere.

4.11 REFINED SPECTROSCOPIC STRUCTURE

A refined spectroscopic information must be utilized in order to do a realistic modeling of radiative transfer. With this need in mind, a computational programming was undertaken which tried to optimize between 2 opposing requirements. On the one hand, the higher the spectral resolution is, written into the program, the more intractable the numerical computation becomes. On the other hand, a simplified spectroscopic representation, although swiftly to handle computationally, removes too much necessary detail.

For our particular simulation of the radiative-conductive-convective heat transfer and the resulting heating/cooling rates, it was decided to adopt for the particular "FLUXOUT" program a spectral increment of 5 cm^{-1}. It is thought that the increment is compatible with the spectral resolution of 2.4 cm^{-1} of the IRIS instrument.

Concerning the complex time-dependent simulation which advances with time steps between 3 and 7.5 minutes and includes solar radiation as well as long-wave radiation, the size of the spectral increment varies between 20 and 50 cm^{-1} in accordance with the fluctuations in numerical value of the spectral parameters. The quasi-random characteristic of the transmission function was maintained.

4.12 WIDTH OF SPECTROSCOPIC RANGE

The total heat transfer simulation performs a full numerical integration over the wave-number range from 200 to about 35,000 cm^{-1}. Some subranges are grouped in which there are only residual intensities either for solar or planetary radiation.

The particular program "FLUXOUT" which attempts to reproduce smoothed IRIS radiance signals from a given temperature sounding input, covers the wave-number range from 200 to 2,000 cm^{-1} in 360 incremental steps.

4.13 INTERACTIONS IN MASTERLOOP

The masterloop of the radiative transfer simulation consists of

- — the cycles through the far IR CO_2 and gray dust absorption band segments,
- — the computation of the layer source functions and transmission functions combined with the gray dust absorption function for 51 layers,
- — the controlling loop applying a product method which relates the respective source layer emission and subsequent attenuations through the intervening layers to the 52 reference levels.
- — the insertion of a fractional reflection of the far IR downward flux components at the lowest reference level (ground surface),

— The computation of the ground flux components received at each level originating from the surface in the far IR band of CO_2 and dust, for each spectral segment and each reference level.

— the collection of ground originating upward flux and contributions to total upward flux at each reference level, for the given band segment,

— the computation of beam transmission functions and dust function for each interval between top of atmosphere and successive reference levels by products, and finally

— the computation of solar flux contributions at each reference level due to direct and ground-reflected insolation for each band segment in near IR bands of CO_2 and dust.

There are various inner loops feeding back into the masterloop at different stages. This structure secures the appropriate interaction between the spectral, the source layer, and reference level domains for solar and planetary , upward and downward radiative fluxes. The analytics to these computational processes have been presented elsewhere (Pallmann, 1968; Pallmann et alii, 1973).

4.14 DISTINCTION BETWEEN COMPONENTS OF GROUND AND ATMOSPHERIC UPWARD FLUX

The attunement of the complete heat transfer model and the separate "FLUXOUT" program is facilitated through numerical information on the separate upward flux components, at the top, for far IR radiation originating at the ground, subsequently attenuated by the intervening atmosphere, and atmosphere originating radiation. As a matter of fact, this distinction between the two components proves to be an excellent simulation tool which afforded us firmer grounds to base our sequential decisions on as regards to which parameters to vary in the simulation sequence and by how much. More specifically, the separate outputs showed how much ground emission is finally coming through the top of the atmosphere as a function of wave-number. The atmospheric component with its spectral dependence over the whole range elucidates the contributions of CO_2 and gray dust from within the band segments to the total upward flux at the top.

4.2 DUST-FREE CASE

The Staff of G.S.F.C. (1973) developed a mean radiance spectrum for the interval from 200 to 2,000 cm^{-1} averaged over 1,842 individual spectra from the RDR records with surface

temperature in the 260-280 K range, and for revolutions later than 100 (3 January 1972). Early timing runs with our "FLUXOUT" program and several temperature sounding inputs appeared promising. Features such as residual water vapor bands in the 200-500 and 1,400-1,800 cm^{-1} regions or silicate sand surface emissions from 900 to 1,200 cm^{-1} are not reproduced for the obvious reason that they were not programmed into the simulation. However, weaker CO_2 bands near 961 and 1,064 cm^{-1} appear as well as the strong CO_2 absorption between 500 and 830 cm^{-1}. Since the fine structure within the CO_2 absorption band about 667 cm^{-1} was reproduced well, it was inferred that the model has a sufficient simulation capability. By feeding the inverted IRIS temperature sounding into the "FLUXOUT" program, one would reproduce the smoothed IRIS radiance signal function within about ± 10% for any running 200 cm^{-1}-segment mean. The integrated deviation amounted to less than 2%.

The curve of the spectral upward flux outside the limits of the 667 cm^{-1}-centered CO_2 band may be approximated by Planck's law (Condon and Odishaw, 1958) expressing the black body flux as a function of wave-number and temperature:

$$(2)\quad F(n;T)\,dn = \frac{2.h.n.^3c^2}{\left(e^{h.n.c/kT}-1\right)}\,du$$

with n: wave-number $\left[cm^{-1}\right]$ and the remaining designations being standard.

A simple conversion of (2) leads to

$$(3)\quad F(n;T)\,dn = \sigma.T.^4 \left[\frac{15\,\pi^{-4}u^3}{e^u - 1}\right].du \text{ with } u = \frac{h.n.c}{k.T}.$$

The fractional factor in brackets is plotted in Fig. 1. The integral of the plotted function over the range $0 \leq u < \infty$ is equal to unity. Equation (3) clearly demonstrates that the black body spectral flux depends on absolute temperature to the fourth power.

In order to indicate the influence of the fractional factor, plotted in the figure, the numerical value of the variable u is given for n = 500 cm^{-1} and T = 250K as 2.88. The plotted curve has its maximum at u = 2.80. It is inferred that equation (3) yields an approximation for the brightness temperature mostly of the ground surface at this particular wave number (see sect. 4.14).

4.3 DUST-LADEN CASE

The method of attunement for the dust-laden case basically utilizes the same model of radiative-conductive-convective heat transfer as before under dust-free conditions except that a dust extinction algorithm is incorporated. Effective dust extinction coefficients are adopted which directly model the radiative absorption capability of the spectrally gray dust particulates. The increase of the radiation mean free path (Zel'dovich & Raizer, 1967) by Mie-type scattering is indirectly simulated through varying the numerical value.

The dependence on altitude of the dust-concentration and the related variation of the dust extinction with height is built into the dust algorithm by the adoption of several vertical profile functions. The two basic analytical forms read as follows:

(4) $EP(I) = EP(52).\exp\left(-A.Z^2(I)\right)$

and

(5) $EP(I) = EP(52).\ \exp\left\{\ 0.0638\left[1-\exp\ (Z(I)/10{,}900)\right].\right.$
$\left.\rho(I)/\rho(52)\right\}$

They represent height-dependent dust extinction coefficients in (cm^{-1}). The variables Z, I, ρ describe height in (m), reference level from the top on down through the range $1 \leqslant I \leqslant 52$, and atmospheric density in ($g.cm^{-3}$). The simulation parameters A and EP(52) are chosen to adjust the profile to what became known of the 1971 dust storm from other Mariner 9 and ground-based observations (See Pang et alii, 1973; Hunt et alii, 1973). In addition, Gierasch and Goody (1972) presented an estimate concerning the effect of dust on the temperature of the Martian atmosphere. This estimate of a 10% absorption by dust is utilized as a criterion for guidance in the simulation procedure. Printouts and plots of atmospheric transparency with respect to ground emission within the interval 200-2,000 cm^{-1} lend themselves to immediate interpretation.

The range of numerical values for EP(52) is from 0.5×10^{-7} to 5.0×10^{-7} cm^{-1}, with the total thickness of

the dust layer varying between 30 and 40 km. The parameter A holds either 1.11×10^{-9} or 4.0×10^{-9} m^{-2}. The dust transmittance is conventionally described by an exponential decline controlled by the optical thickness. The profile for the dust extinction coefficient as stated in equation (5) is the same as that discussed by Conrath (1974) if one inserts for the effective "top" of the dust layer 30 km and for the pressure scale height 10.9 km.

Heuristic simulation runs indicate that for these particular values a profile shape results which may more easily be described by a Z^2-function. Furthermore, the delayed reduction of the dust coefficient in the vicinity of the surface approximates the effect of convective mixing on the vertical distribution of dust. The time-dependent radiative-convective heat transfer model generates buoyant convection in the lowest 5,000-7,000 m also if dust is present.

Finally, a summary of the simulative attunement is given. First, the radiative-conductive-convective model generates, after completion of a balanced diurnal cycle, a temperature profile for the particular hour of the IRIS scan. This profile is used as an input in the "FLUXOUT" program which simulates spectral upward fluxes in the interval 200-2,000 cm^{-1}, checked at the "top" of the atmosphere. Then a computational comparison is made between the IRIS radiance data and the simulated flux values.

Subsequently, a closer fit is generated by a variational simulation with respect to temperature input and dust extinction function. By incorporating a T-profile modifier, the program lowers temperatures below 15 km or 25 km while increasing them above. This procedure readily demonstrates the control which the thermal fields of the lower and upper atmospheric layers have as regards to the upward flux at the top. After repeating this procedure with different dust and temperature profiles, the attunement of the computer model is considered approximate. It is inferred that among all pairs of dust- and T-profiles, used in the procedure, that pair is optimal which complies with most of the criteria controlling the simulation. In conclusion, the best-fit T-profile which has 11 data points below 6 km and 41 more up to the top of the atmosphere, represents the amended temperature sounding to replace the IRIS inverted profile.

5.0 DISCUSSION OF RESULTS

The computer simulation attuned to IRIS radiance signal functions generated an extensive output of which a smaller selection will be discussed here. Two different programs were utilized to create outputs, i.e., (1) the "FLUXOUT" program (henceforth called the F/O-Model) which simulated for the particular days and hours of the Mariner 9 IRIS scans the spectral upward flux originating at the surface and 51 atmospheric layers, and (2) the high time-resolution radiative-conductive-convective heat transfer model (henceforth called the RCC-Model) which generated the balanced diurnal cycle with time-steps from 3 to 10 minutes.

Planetary radiation transfer under dust-free conditions is easily discussed by utilizing the Planck-Stefan-Boltzmann law of black radiation in the form given by equation (3) and the plot in Fig. 1. The T^4-dependence clearly indicates the high degree of sensitivity to temperature changes held by the upwardly directed radiative flux. The surface temperature essentially controls the general shape of the spectral flux curve outside the limits of the CO_2 absorption band near 667 cm^{-1}.

Concerning dust-laden conditions, the particular IRIS scan of Dec. 3, 1971 at 16.23 Local Martian Solar Time (LMST) is chosen for discussion. Table 1 presents the basic

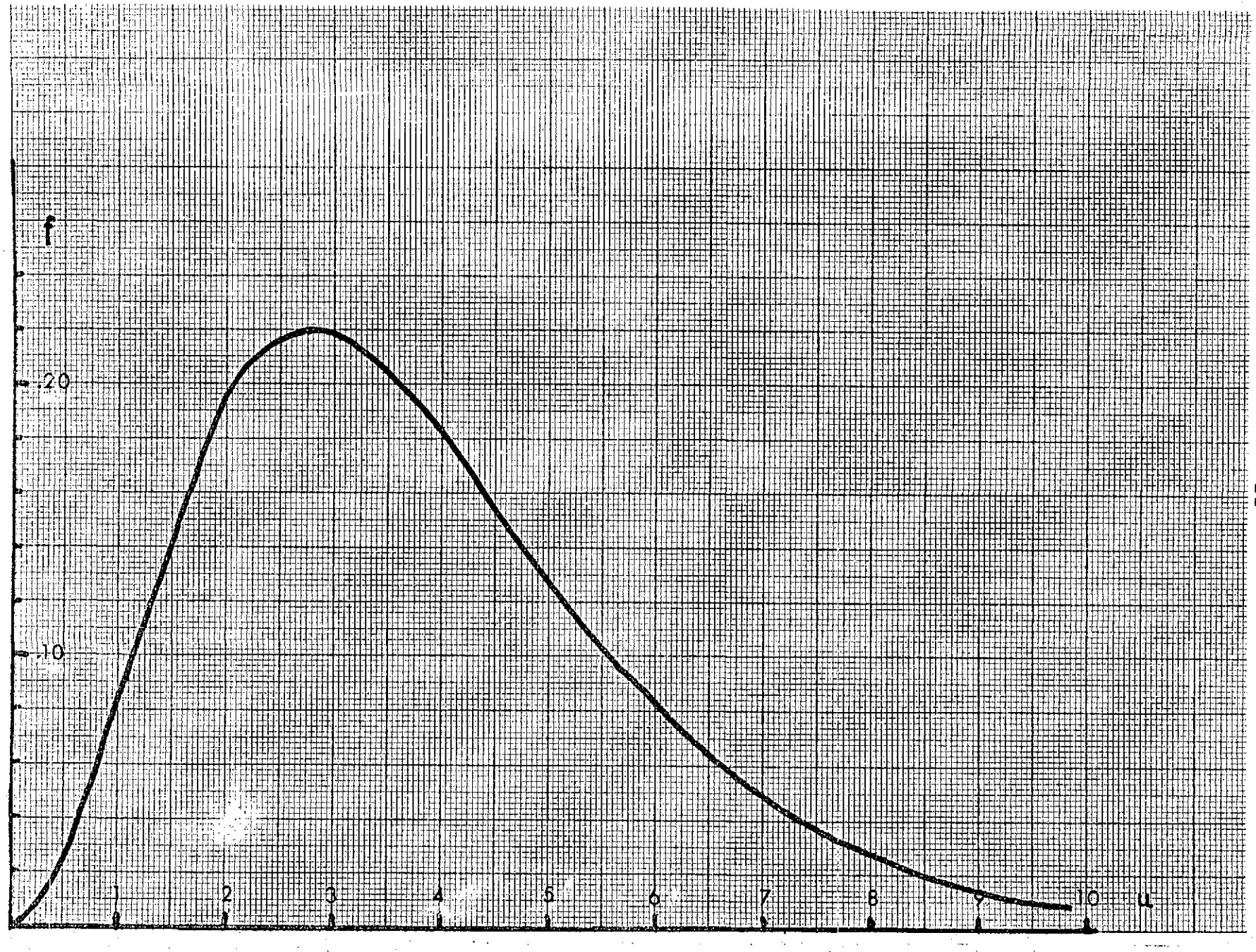

Fig. 1: Plot of fractional factor $f(15.\pi^{-4}.u^3)/(e^u-1)$ vs. $u=(h.n.c)/(k.T)$, with n:wave-number in cm^{-1}.

MARTIAN ATMOSPHERE RAD*COND*CONV HEAT TRANSFER

SIMULATION

BASIC PARAMETERS

Initial Time	16.23 Local Martian Solar Time
Number of Time Steps	288
Timestep Interval	1o min (Martian)
Surface Albedo	.3
Soil Density	1.7
Soil Conductivity	6.27 E 03
Soil Heat Capacity	1.003 E 07
Surface Emissivity	1.000
CO_2-gas conductivity	1.330 E 03
Latitude	-42.31
Declination of sun	-20.370
Duration of sunshine	878.03 min (Martian)
Ratio of Mean/Actual solar distance	1.0655

1 Martian solar day - 24 Martian hours - 1440 Martian min

all units in cgs unless otherwise noted

TABLE 1

parameters of the scan. In Fig. 2, the spectral upward flux at the top of the atmosphere is presented as a function of wave-number. The attuned F/O-Model generated an output relatively close to the IRIS signal function. Since the inverted IRIS temperature sounding is used as input, the plot demonstrates the capability of the F/O-Model to reproduce the signal function under dust-laden conditions. The applied dust extinction function reads EP(I) = 5.8646E-8*EXPF (-4.E-9*Z(I)* Z(I)).
(See eq. (4)).

As shown in Fig. 3, the ground emission is the predominant feature among the atmospheric and ground flux components except for the CO_2 absorption band near 667 cm^{-1}. Attention is called to the wings of the band. While the ground flux is diminishing, the atmospheric layer contributions take over at a higher thermal level. In the center of the band, no ground flux is registered at the top of the atmosphere. This behavior of atmospheric attenuation of the ground emission is demonstrated in Fig. 4, which presents the atmospheric transparency as a function of wave-number.

The dust extinction coefficient in cm^{-1} is plotted in Fig. 5. Curve A represents the chosen Z^2-profile whereas curve B is a profile structured in accordance with an analytical expression given by Conrath (1974). Although the two profiles appear different, they do not generate any

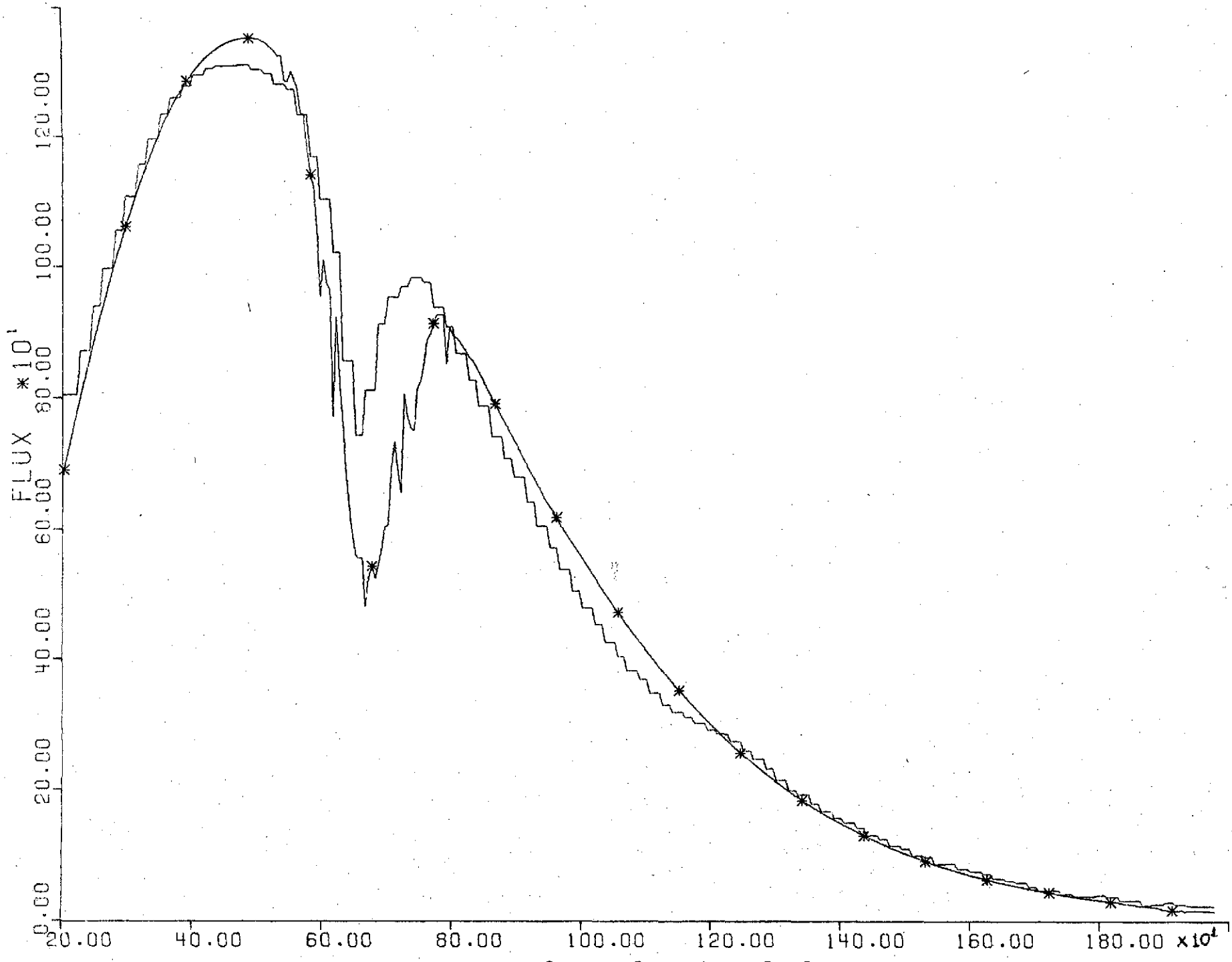

Fig. 2: Spectral upward flux in erg. cm^{-2} sec^{-1}. $(5\ cm^{-1})^{-1}$ at the top of the atmosphere versus wave-number in cm^{-1}. The stepped curve is the smoothed IRIS radiance signal function converted to flux; the starred curve is the sinulated output with the inverted IRIS T-profile as input. IRIS scan taken on Dec. 3, 1971 at 16.23 LMST.

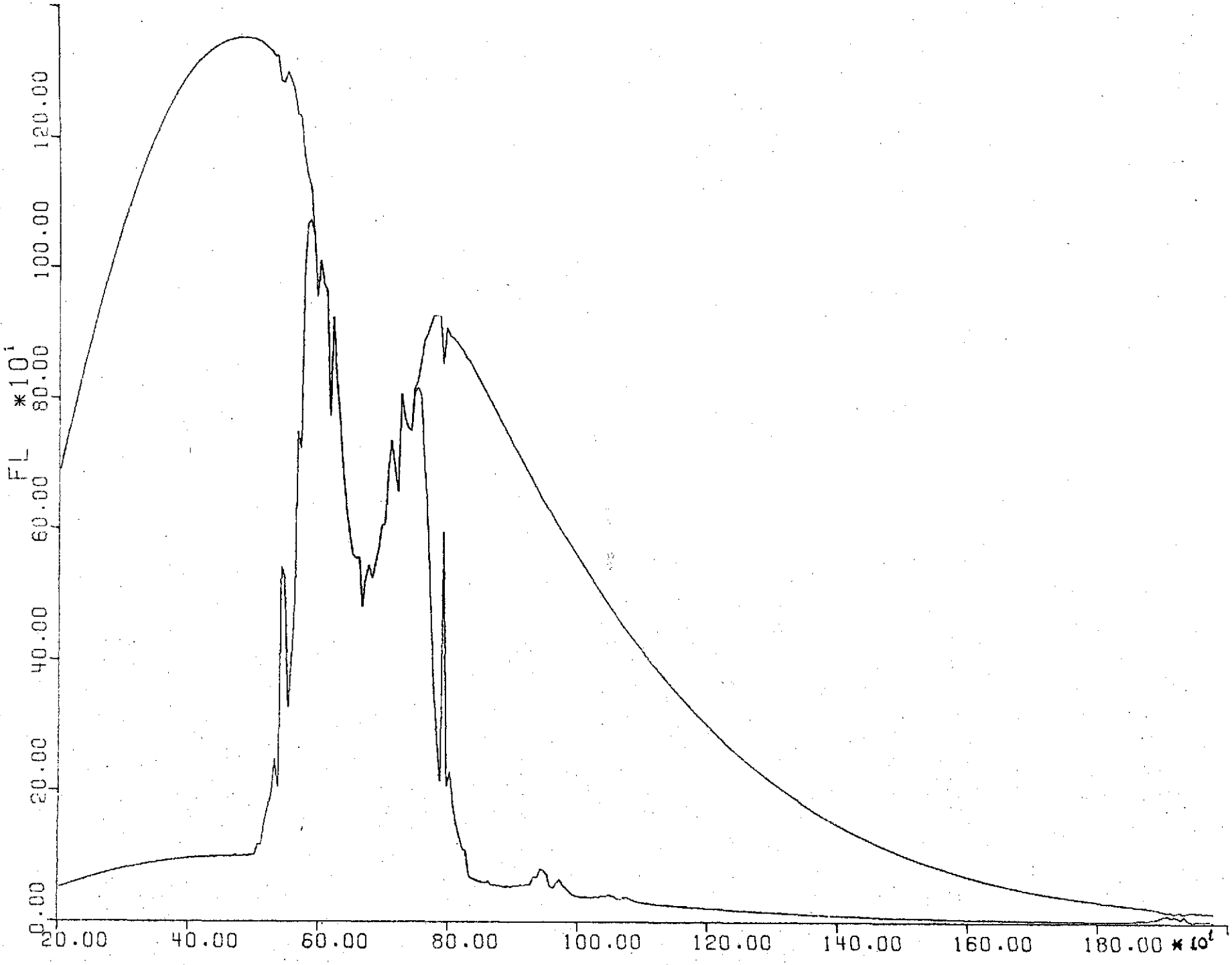

Fig. 3. Simulated spectral upward flux components; upper curve same as in Fig. 2 representing upward flux total composed of residual from ground and strictly atmospheric contribution (lower curve).

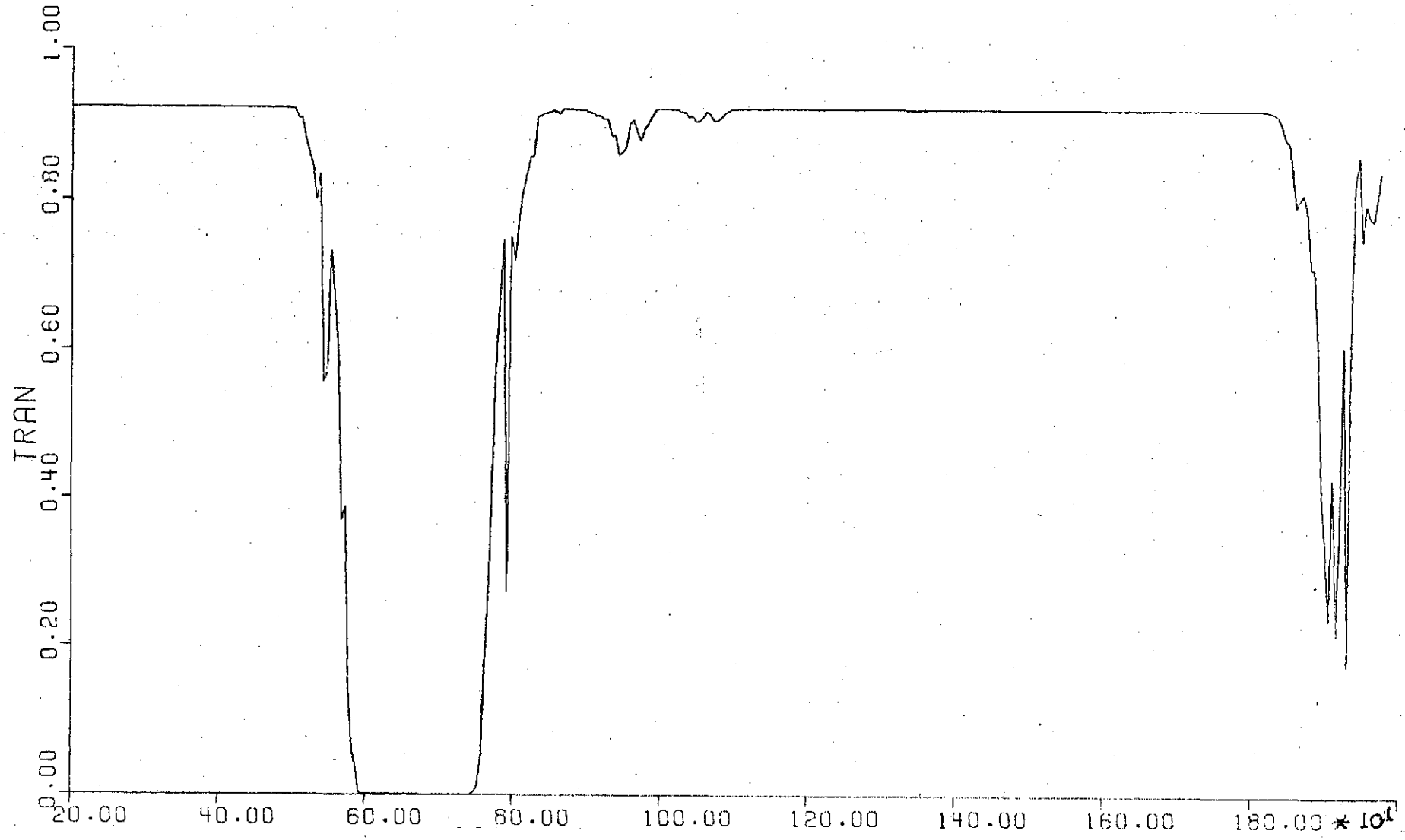

Fig. 4: Transparency of atmosphere to ground emission vs. wave-number in cm^{-1}. Same conditions as in Fig. 2.

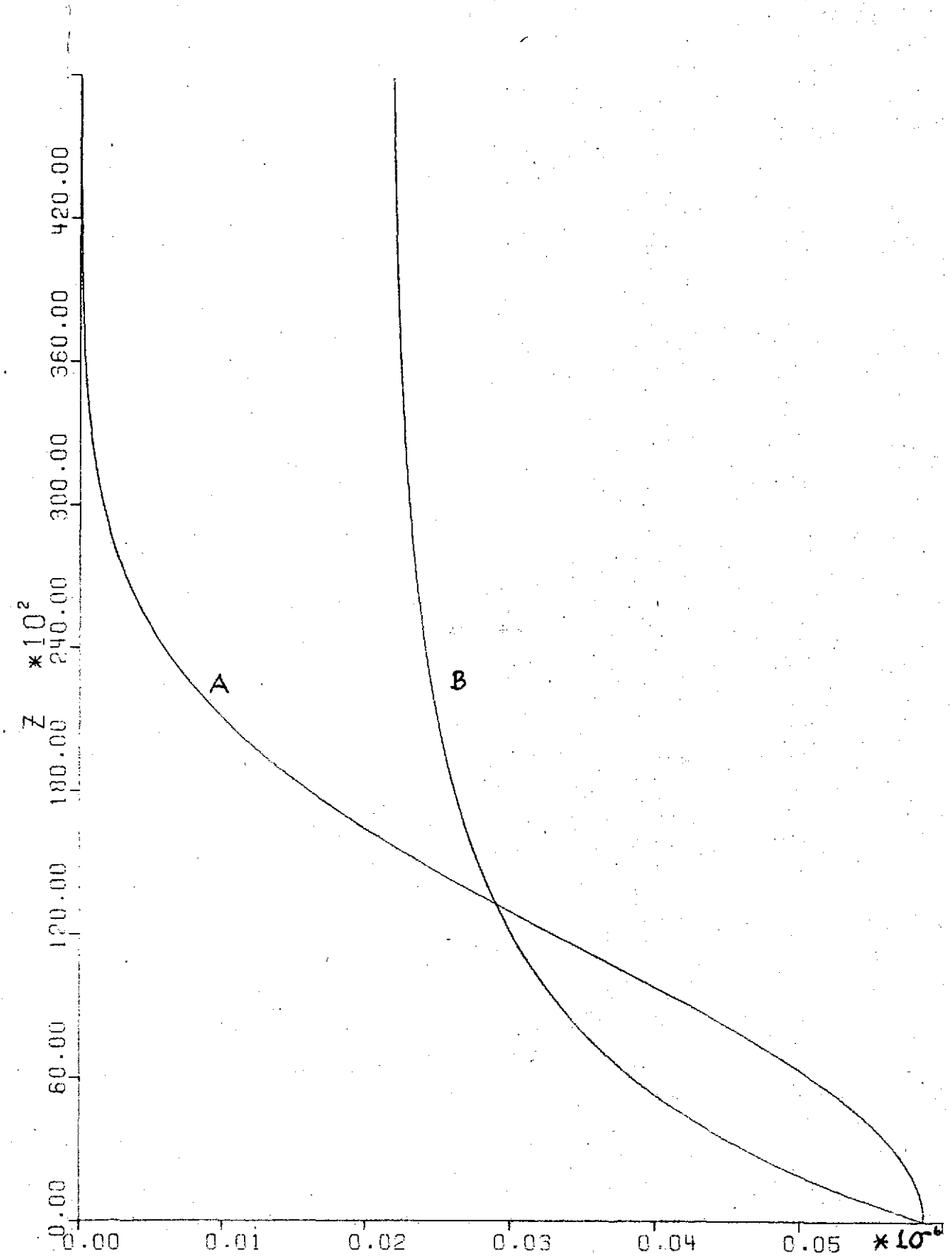

Fig. 5: Dust extinction coefficient in cm^{-1} vs. height Z in 10^2 m. Curve A: Z^2-profile; curve B: Conrath-profile. Same conditions as in Fig. 2.

appreciable difference in upward flux components and transparency. It is the numerical value of the profile amplitude at the ground which counts.

In Figs. 6 - 10, the results of a second phase of simulation are discussed. In this phase, an improved temperature stratification was derived to be used as the particular T-sounding input for the F/O-Model. The optimal temperature modifier proved to be T(IAS) = T(IAS) - T(IAS)/10. * (1 - Z(IAS)/15000.) which was applied to the interim T-profile generated by the RCC-Model in the balance of diurnal cycle.

The particular dust extinction function for the second phase of simulation has 1.5×10^{-7} cm^{-1} as its amplitude value EP(52) with A being 1.11×10^{-9} m^2. The height of the dust layer is optimized to 40 km (See Fig. 9). At this level, the dust extinction coefficient is still about 18% of that near the surface. Furthermore, the Gaussian structure of the curve more realistically models the effect of convective mixing on the vertical dust transport. Convection appears to be activated between mid-morning and early afternoon. Thus, one can expect a rather constant vertical dust distribution in the lowest 5 - 7 km. If there is no dust, convective overturn extends up to 13 km for the particular values of time of the Martian year and latitude given by the IRIS scan.

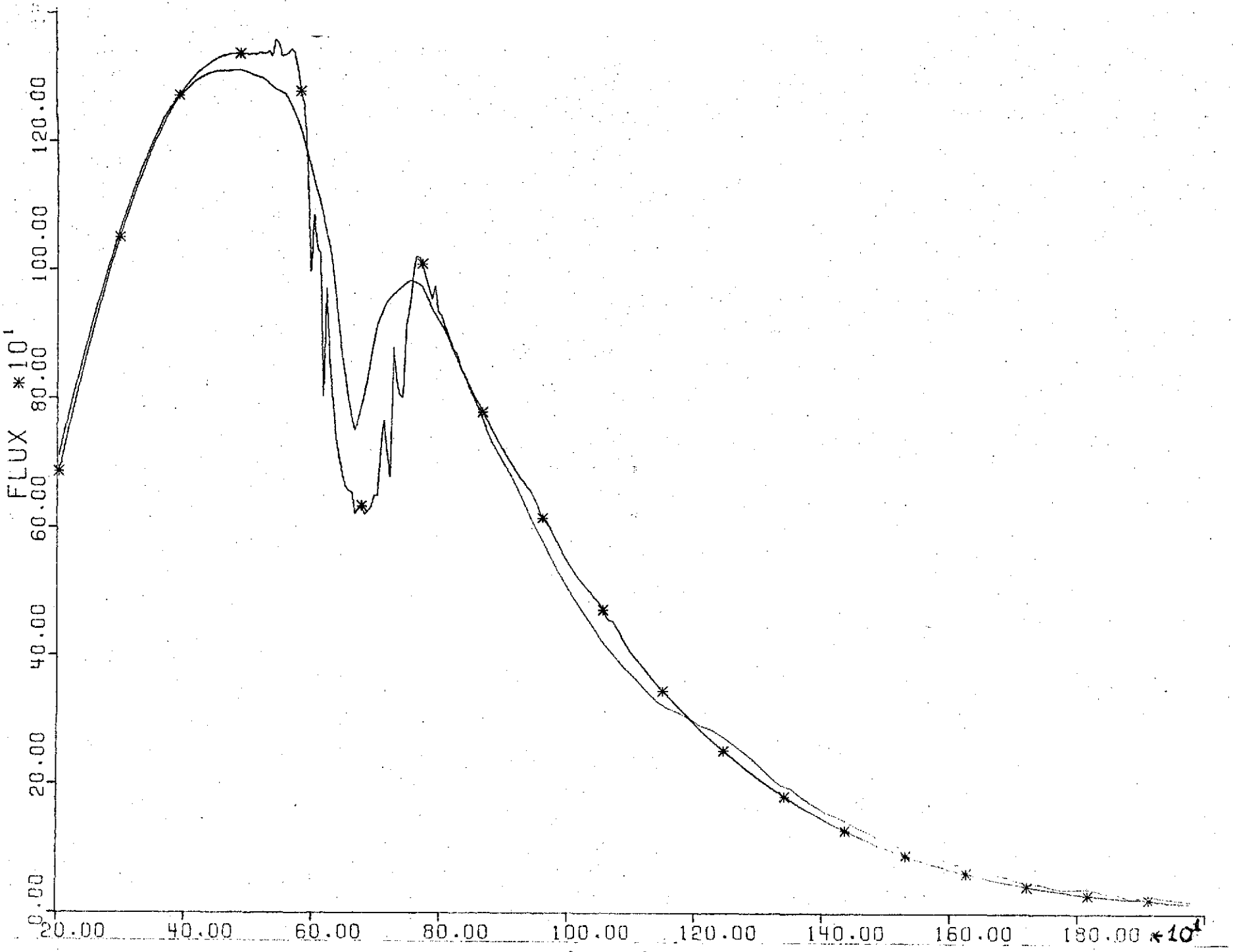

Fig. 6: Spectral upward flux in erg. cm^{-2} sec^{-1}. $(5cm^{-1})^{-1}$ at the top of the atmosphere versus wave-number in cm^{-1}. Same as Fig. 2 except for dust function (see Fig. 9).

As an additional phenomenon in the second simulation phase, an 8-km deep convective layer appears near the top of the dust "table" (40 km). As a matter of fact, this layer persisted longer than that near the ground surface. Thus, an abrupt decline of dust concentration seems to be conducive to the generation of a free-atmospheric convection layer. This result confirms a finding presented by Dannevik and Pallmann (1974; see Appendix).

In Fig. 7, the spectral flux components of ground emission and atmospheric contribution are given pertaining to the second simulation phase. The atmospheric transparency to upward ground flux is presented in Fig. 8. Outside the limits of the CO_2 absorption band, dust absorbs totally about 22% of the short- and long-wave radiation coming into the atmospheric layers from top and bottom. For the particular dust extinction coefficient, see Fig. 9. The pertinent temperature sounding simulated by the F/O-Model is shown in Fig. 10. As previously stated, a particular modifier is applied facilitating further decision-making in the procedure as well as developing that kind of T-sounding which is judged to improve on the IRIS inverted temperature profile in the presence of dust. It is thought that the thin solid curve represents such an improvement for the particular date and hour. For comparison, the inverted IRIS sounding (dashed curve) and the simulated

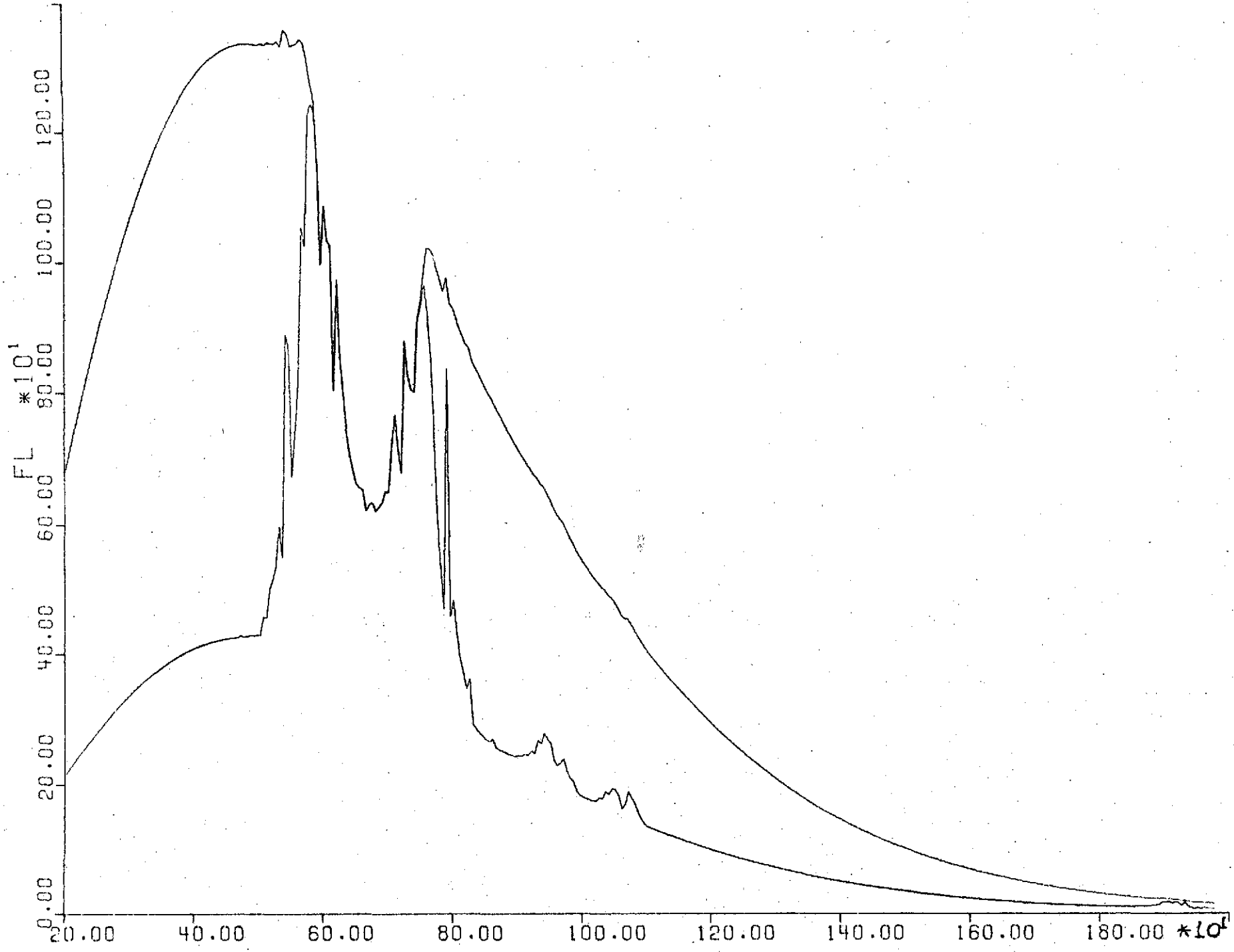

Fig. 7: Same as Fig. 3 except for dust function (see Fig. 9).

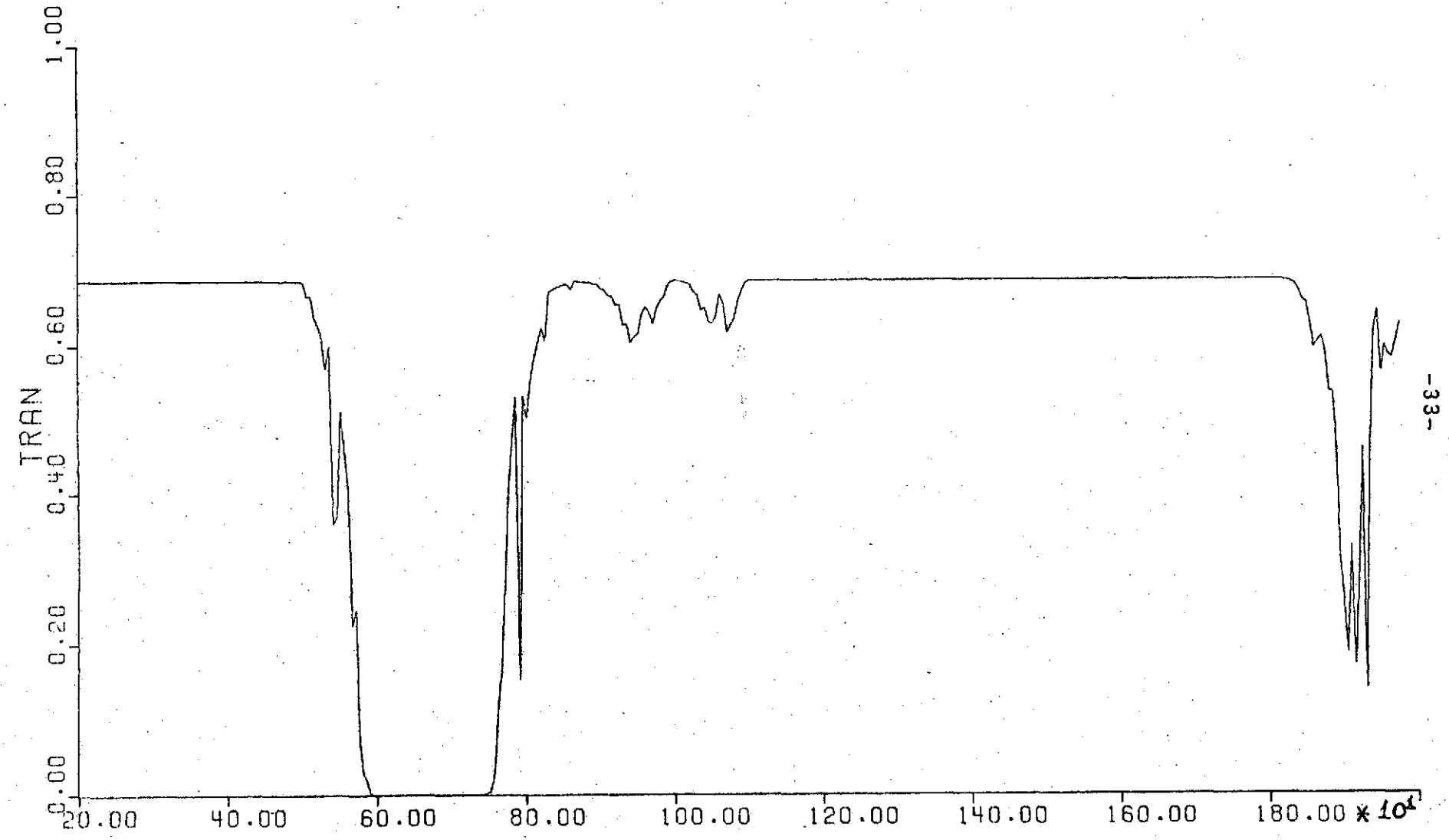

Fig. 8: Same as Fig. 4 except for dust function (see Fig. 9).

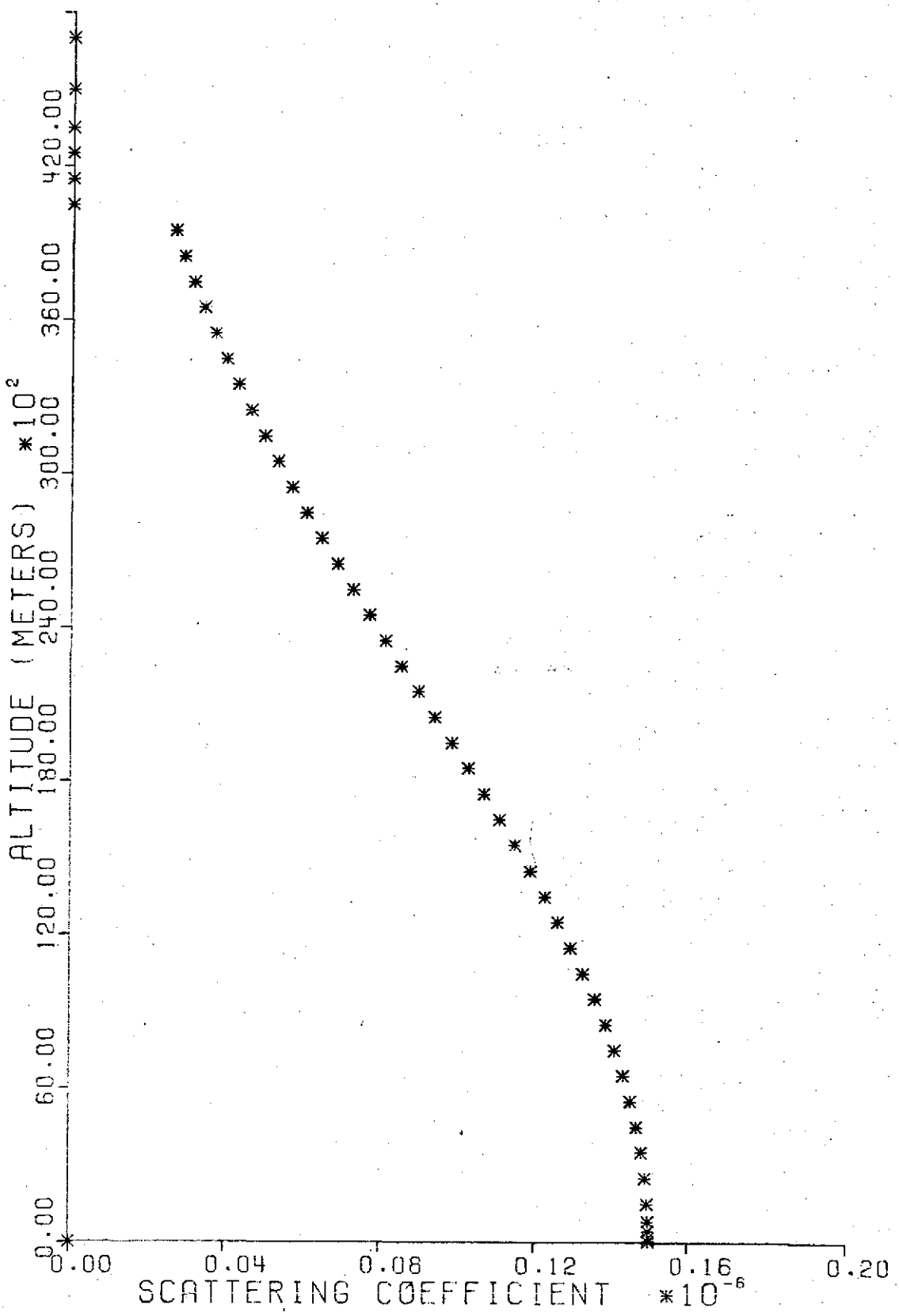

Fig. 9: Dust extinction coefficient in cm^{-1} vs. altitude in 10^2 m. Height of dust layer top: 40 km. Same conditions as in Fig. 6.

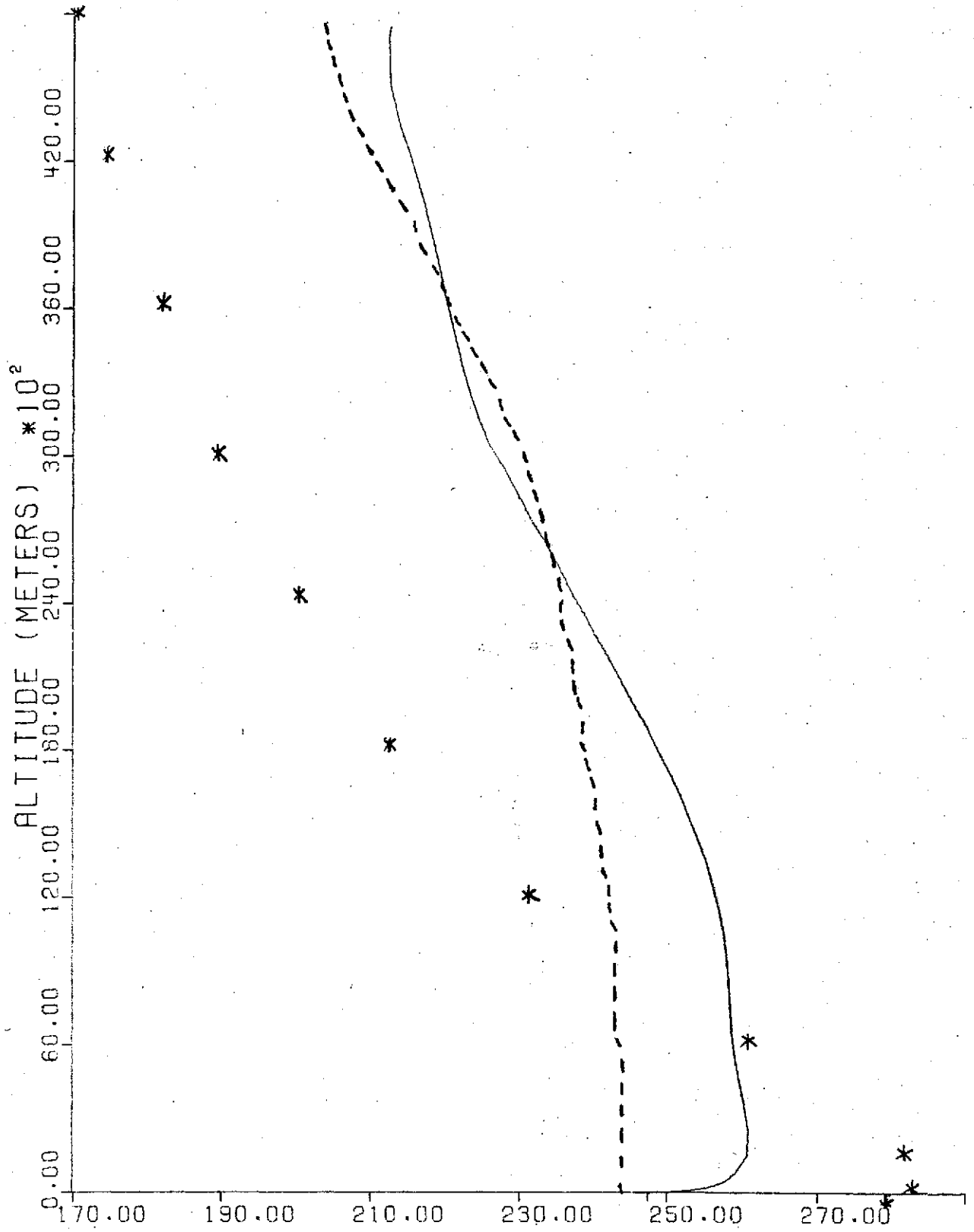

Fig. 10: Simulated temperature sounding in ^{o}K versus altitude in 10^2 m. The applied modifier is T(IAS) = T(IAS) - T(IAS)/10.*(1-Z(IAS)/15000.) ; starred curve shows dust-free profile for Dec. 3, 1971; dashed curve: inverted IRIS sounding of same data.

profile for dust-free conditions (starred curve) are given. The mathematical inversion technique fails to bring out any surface temperature inversion which amounts to about 15°K for the modeled profile (solid curve). The spatial resolution of the inverted profile is about 6 km near the surface (Conrath, 1972; Pearl, 1974), whereas the present technique offers 11 data points within this height interval. Also, the modification by dust in the vertical redistribution of heat by radiative and convective transports was not built into the inversion method.

A few preliminary results of a third simulation phase are offered. This phase deals with improving the RCC-Model. The particular refinements are: (1) a 5% diffuse reflection capability for each of 5 layers (1000 m thick) from the top of the dust "table" on down; (2) a weaker dust extinction, i.e., EP(I) = 5E-7* EXPF(-1.11 E-9 * Z(I) * Z(I)); (3) a sand surface albedo of 0.3; (4) a long-wave emissivity of 0.9 at the sand surface (Hellespontus); and (5) the temperature profile of Fig. 10 (solid curve) as input. A diurnal cycle balance was achieved.

In Fig. 11, the RCC-Model generated spectral flux components are given for the same date as before. Although some improvement was achieved, the ground emission is still too large. However, the direction in which further refinement has to go is quite clear. The dust extinction function

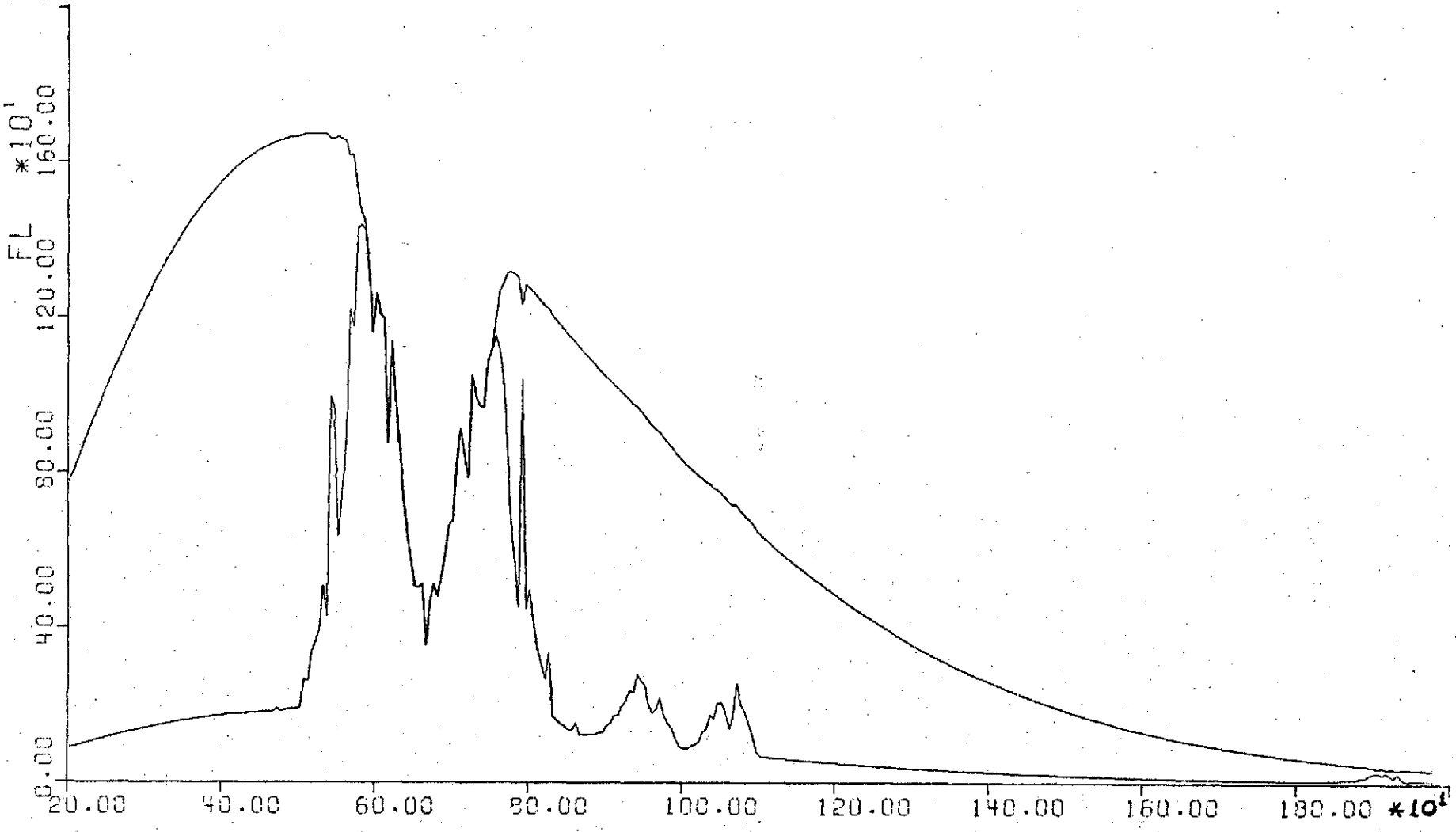

Fig. 11: RCC-Model generated spectral flux components; upper curve: Upward flux total composed of residual from ground and strictly atmospheric contribution (lower curve). Date: Dec. 3, 1971; 16:23 LMST.

of Fig. 12 applied in the RCC-Model is a result found after several simulative steps were undertaken. It appears that higher dust concentrations produce an intense warming in the atmosphere between 5 and 25 km.

The RCC-Model generated T-soundings are examplified in Fig. 13. From a comparison between various profiles of the same date, it is evident that the refinements performed in the third simulation phase are very promising. Mostly the ground-atmosphere interface physics needs additional attention. It is concluded that the F/O-Model-and RCC-Model-generated temperature profiles render a sufficient basis for reinterpreting the IRIS inverted T-soundings.

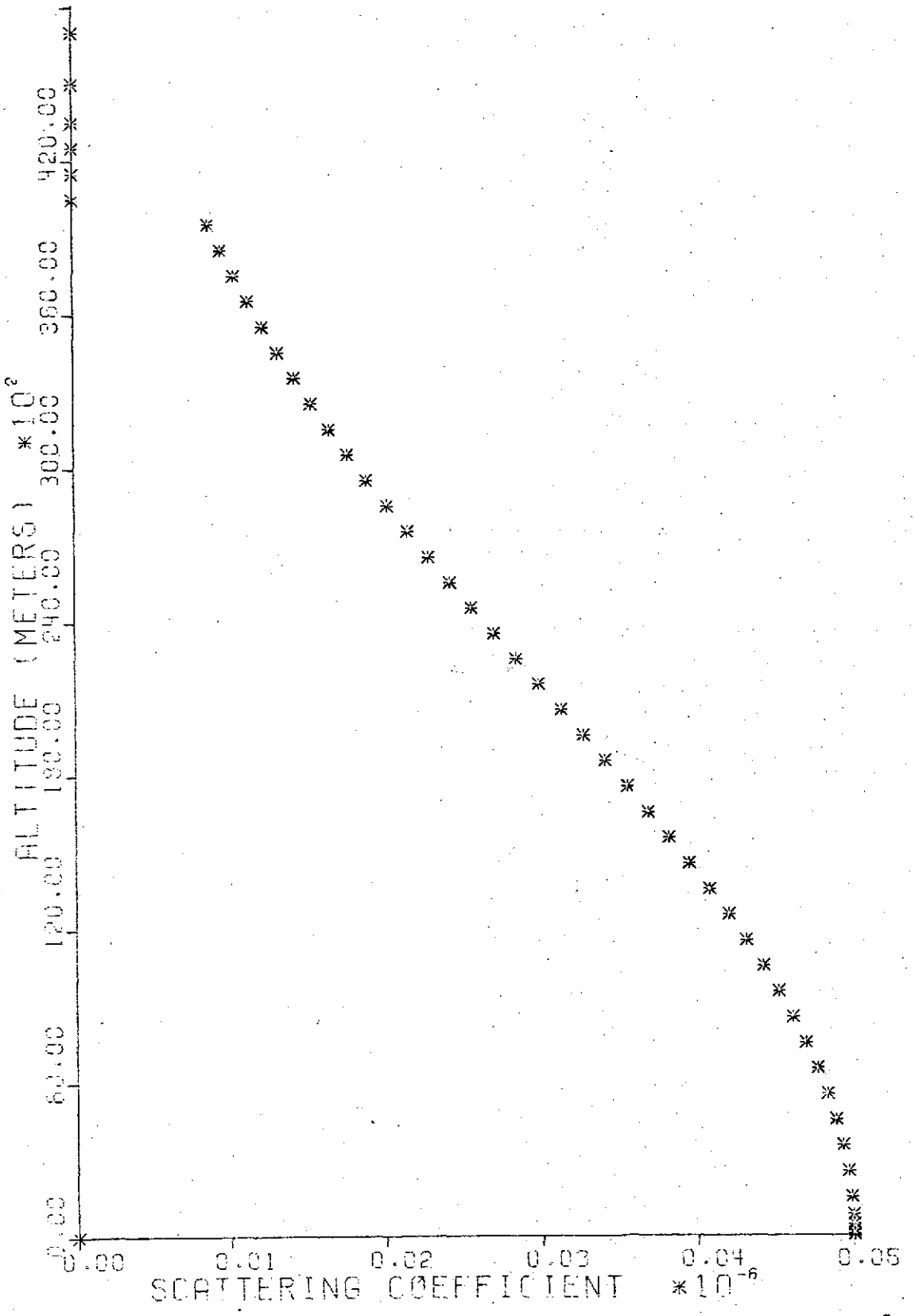

Fig. 12: RCC-Model dust extinction coefficient in cm^{-1} vs. height Z in 10^2 m.

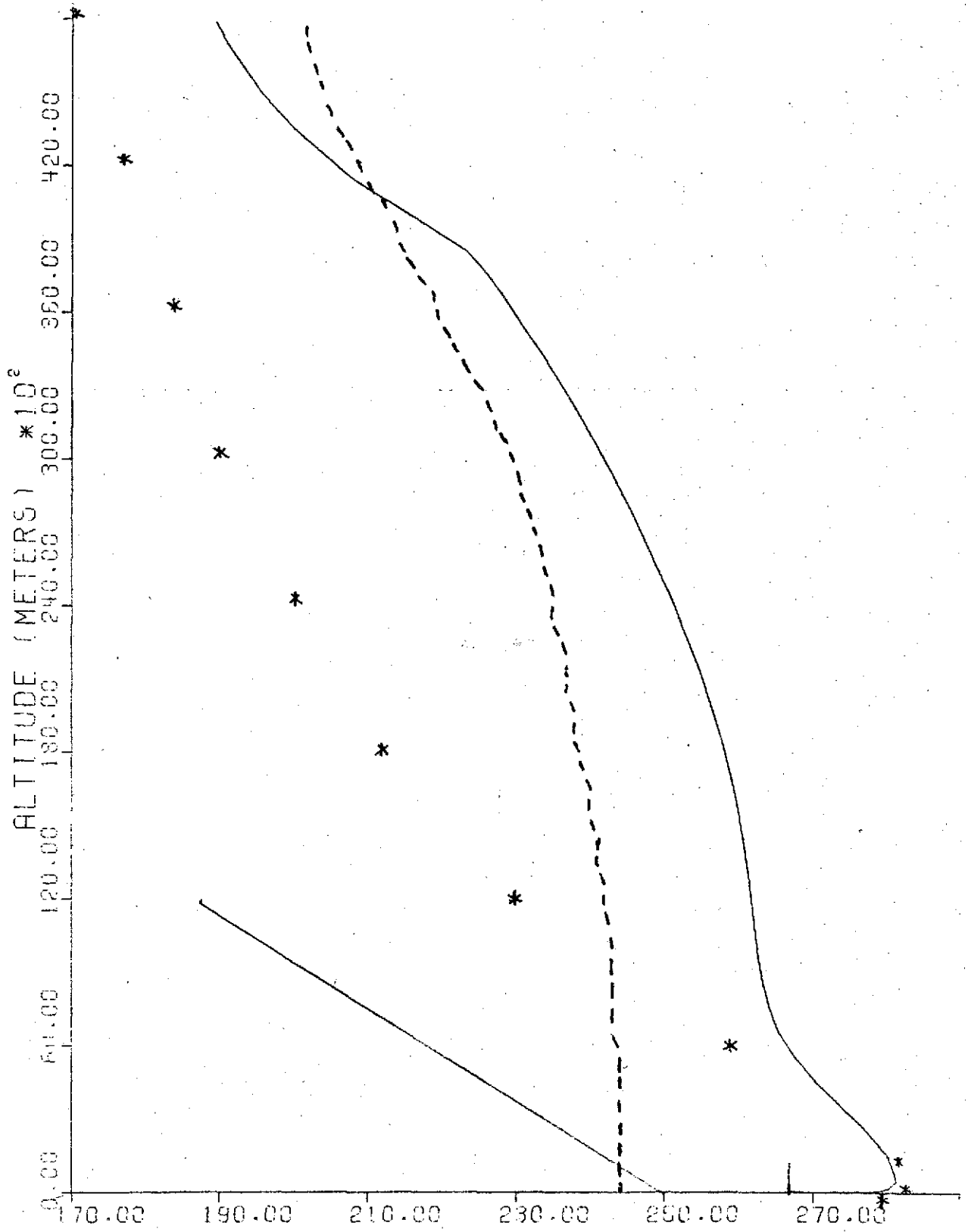

Fig. 13: RCC-Model generated temperature sounding in °K for balanced diurnal cycle (thin solid curve); inverted IRIS sounding (dashed curve); CO_2 adiabat (straight line); dust-free sounding (asterisks); date: Dec. 3, 1971, 16.23 LMST.

6.0 SUMMARY OF FINDINGS

As discussed in sections 2.0, 3.0, and 4.0, a previously developed model was refined and attuned to Mariner 9 IRIS radiance data. Extensive outputs were generated by the attuned model establishing an adequate basis to formulate inferences into the degree of representativeness of IRIS inverted temperature soundings. Some of the more basic results developed by means of systematic numerical experiments with the model are:

(1) In the presence of little dust within the mid-latitudinal Martian atmosphere, strong-line radiative communication from the ground, supported by convective-conductive heat transfer, generates a thermal structure in the lowest 8-13 km, which is highly dependent on the hour of the day. The diurnal temperature oscillation at the ground is about 110°K and at 10 km still close to 15°K.

(2) Under the same condition as in (1), weak-line radiative communication by the ground reaches beyond 25 km maintaining a diurnal T-oscillation of several degrees. There is some heat exchange with outer space. The uppermost regime (40-50 km) is under the predominant control of the upper boundary.

(3) If the atmosphere sustains an optically-thick dust layer, strong-line radiative transfer supported by convection produces greater thermal variations only in the lowest 4-6 km. The diurnal temperature oscillation at the ground is about 90°K.

(4) In the presence of thick dust, weak-line radiative communication between ground and atmosphere causes intense heating from 5-25 km. At the top of the dust layer a several km thick convective layer is generated if dust concentration decreases rapidly at the "top". It will last for several hours .

(5) Mid-latitudinal IRIS inverted temperature sounding for the dust-laden phase of the Mariner 9 mission deviate from the fine structure of the T-profile, especially in the lowest 6 km, produced by the attuned F/O- and RCC-Models. It is concluded that lack of spatial resolving power and insensitivity to time-dependence, inherent in the IRIS inversion technique and the mode of measurement, introduce in the inverted profiles a discrepancy which may be overcome by adopting some of the presented findings.

REFERENCES

Conrath, B. J., 1972: Vertical Resolution of Temperature Profiles Obtained from Remote Radiation Measurements. Journal of the Atmospheric Sciences, 29, 1262-1271.

_____, 1974: Thermal Structure of the Martian Atmosphere During the Dissipation of the Dust Storm of 1971. NASA Goddard Space Flight Center, X-622-74-111. Greenbelt, Maryland. 33 pg.

Dannevik, W. and A. J. Pallmann, 1974: Mariner-9-Based Simulation of Radiative Convective Temperature Changes in the Martian Dust-Laden Atmosphere-Soil System. Accepted for publication in Rivista Italiana di Geofisica.

Drayson, S. R., 1972: Atmospheric Radiative Transfer by Carbon Dioxide. Preprints from Conference on Atmospheric Radiation, Fort Collins, Colorado, Aug. 7-9, 1972. 77-79, American Meteorol. Soc. .

Gierasch, P. J. and R. M. Goody, 1972: The Effect of Dust on Temperature of the Martian Atmosphere. Journal of the Atmospheric Sciences, 29, 400-402.

_____, 1973: A Model of a Martian Great Dust Storm. Journal of the Atmospheric Sciences, 30, 169-179.

Goody, R., 1964: Atmospheric Radiation. Clarendon Press, Oxford. 436 pp.

Hanel, R. et alii, 1972: Infrared Spectroscopy Experiment on the Mariner 9 Mission: Preliminary Results, Science, 175, 305-309.

Hess, S. L., 1973: Martian Winds and Dust Clouds. Journal of Planetary and Space Science, 21, 1549-1557.

Hunt, G. R. et alii, 1973: Mars: Components of Infrared Spectra and the Composition of the Dust Cloud. Icarus, 18, 459-469.

Kraichnan, R. H., 1959: Structure of Isotropic Turbulence at Very High Reynolds Numbers. J. Fluid Mechanics, 5, 497-515.

McClatchey, R. A. et alii, 1973: AFCRL Atmospheric Absorption Line Parameters Compilation. AFCRL-TR-73-0096, 78 pp.

Pallmann, A. J., 1968: Radiative Heating and Cooling Functions for the Lower Martian Atmosphere Under the Condition of Local Thermodynamic Equilibrium (LTE). NASA Publ. CR-1044, VIII + 40 pp.

_____ and S. P. Frisella, 1972: Numerical Simulation of Radiative-Conductive Heat Transfer in the Martian Atmosphere-Polar Cap Utilizing Mariner 9 IRIS Data. Preprints from Conference on Atmospheric Radiation, Fort Collins, Colorado, Aug. 7-9, 1972; 292-295, American Meteorological Society.

_____ and W. P. Dannevik, 1972: Transient Variation of Martian Ground-Atmosphere Thermal Boundary Layer Structure. Preprints from Conference on Atmospheric Radiation, Fort Collins, Colorado. Aug. 7-9, 1972; 288-291; American Meteorological Society.

_____ et alii, 1973: Martian Thermal Boundary Layers: Subhourly Variations Induced by Radiative-Conductive Heat Transfer within the Dust-laden Atmosphere-Ground System. NASA Publ. CR-2318; XI + 83 pp.

Pearl, J., 1974: Personal Communication.

Staff, of G.S.F.C., 1973: Mariner 9 IR Interferometer Spectrometer (IRIS) Reduced Data Records Documentation. NASA Goddard Space Flight Center, X-622-73-305. Greenbelt, Maryland. 17 pp. + App's.

_____, 1973: Mariner Mars 1971 Project Final Report. TR-32-1550, Vols. IV and V. Jet Propulsion Lab, Pasadena, California.

Zel' dovich Y. B. and Raizer, Y. P., 1967. Physics of Shock Waves and High Temperature Hydrodynamic Phenomena. Vols. I and II. Academic Press, New York, 464 and 452 pp.

APPENDIX

Research Paper

by

Dannevik, W. P. and A. J. Pallmann, 1974:

Mariner-9-Based Simulation of Radiative-Convective Temperature Changes in the Martian Dust-laden Atmosphere-Soil System.

Accepted for publication in Rivista Italiana di Geofisica (Editor: Prof. Dr. M. Bossolasco)

MARINER-9-BASED SIMULATION OF RADIATIVE CONVECTIVE TEMPERATURE CHANGES IN THE MARTIAN DUST-LADEN ATMOSPHERE-SOIL SYSTEM

William P. Dannevik and Albert J. Pallmann

Division of Atmospheric Science

Saint Louis University, Missouri 63103

January 1974

Abstract

A numerical simulation of radiative, conductive, and convective heat transfer of the Martian dust-laden atmosphere-soil system is presented with particular emphasis given to heating/cooling in regions of sharp variation in temperature or absorption and its resultant impact on outgoing planetary spectral radiance, as measured by the Mariner 9 IRIS. Thermal coupling between the ground and atmospheric subsystems is modeled by the total heat flux balance at the interface. In the simulation procedure, local thermodynamic equilibrium (LTE) is assumed, and a combined strong-weak line transmission function permits short- and long-range exchanges of energy from the surface toward space. Direct absorption of insolation in the near-IR bands by both silicate dust and CO_2 is incorporated. The thermal coupling appears as a boundary-initial value problem which has been solved through forward-time integration in 15-minute steps. The input data base stems from various experiments flown on Mariner 9. Results of interest are: (1) atmospheric counter-radiation is increased by more than 50% in the presence of dust, (2) tropospheric convective mixing is confined to the lowest 5 km, (3) quasi-isothermal stratification results in the upper part of the dust layer during the period of intense solar heating, (4) a highly effective radiation-convection layer exists at the top of the dust stratum with a diurnal temperature variation of 40 K.

Zusammenfassung

Eine numerische Simulation des Wärmetransports durch Strahlung, Wärmeleitung und Konvektion in dem staubgeladenen Atmosphäre-Boden System des Planeten Mars wird vorgelegt, die insbesondere Erwärmung und Abkühlung in den Bereichen scharfer Änderung der Temperatur oder Absorption berücksichtigt mit dem sich daraus ergebenden Einfluss auf die aufwärts gerichtete, planetarische, spectrale Radianz, wie sie durch Mariner 9 IRIS gemessen wurde. Die thermische Koppelung zwischen dem Boden und dem atmospharischen System ist modellmässig gegeben durch die Bedingung der Kontinuität des totalen Wärmeflusses an der Zwischenfläche. Der Modellierungsvorgang sieht lokales thermodynamisches Gleichgevicht (LTE) vor; eine kombinierte Transmissionsfunktion für starke und schwache Absorptionslinien erlaubt Energieaustausch über kurze und weite Distanzen vom Boden bis zu grossen Höhen. Ausserdem ist direkte Absorption der Sonnenstrahlung im nahen Infrarot einbezogen für Silikatstaub und Kohlendioxyd. Die thermische Koppelung stellt sich als Grenz-Anfangswert-Problem dar, das durch Vorwärtsintegration in 15-Minuten Intervallen gelöst worden ist. Die Eingabedaten stammen von verschiedenen Experimenten, die mit Mariner 9 geflogen wurden. Ergebnisse von Interesse sind: (1) atmosphärische Gegenstrahlung nimmt um mehr als 50% zu, wenn Staub gegenwärtig ist; (2) troposphärisch-konvektive Mischungsvorgänge sind auf die untersten 5 km beschränkt; (3) quasi-isothermische Schichtung ergibt sich im oberen Teil der Staubschicht während der Zeitspanne intensiver solarer Erwärmung; (4) eine Schicht hochwirksamer Strahlungsdivergenz und Konvektion existiert an der Obergrenze der Staubschicht, die eine ganztägige Temperatur-schwankung von etwa 40°K aufweist.

1. Introduction

The global extent of sand-like dry soil material on Mars permits the surface temperature field to respond rapidly to changes of largely-unattenuated insolation, with the mid-latitudinal diurnal variation being $\sim 70K$. In addition, the predominance of CO_2 and relative tenuity of the Martian atmosphere result in a large radiative response capability; therefore, a significant diurnal thermal boundary layer is induced even if convection were absent. Analysis of radiative relaxation times for Mars (Goody and Belton, 1967) indicates a characteristic depth of 1.6 km for the diurnal temperature wave. The latter study also shows that molecular conduction may be an important transfer mechanism for thermal perturbations of spatial scale $< O(10m)$.

The purpose of this note is to present some first findings of a numerical modeling developed to (1) investigate the thermal coupling of the Martian atmospheric and soil subsystems, and the resultant diurnal temperature variation in the lowest scale-heights of the atmosphere and (2) develop some criteria for the interpretation, under the condition of atmospheric dust loading, of Mariner 9 IRIS inverted data.

The design of the numerical model departs in several essential ways from that employed by Gierasch and Goody (1967, 1968). In the latter model, a "trapozoidal rule" was used to approximate the exchange integral for planetary radiative

heating, correctly accounting for the boundary terms while representing the contribution from various atmospheric source layers with emission terms evaluated at two discrete points which are sometimes far apart. This approximation emphasizes the long-range exchange but eliminates the effects of short-path, strong-line radiative transfers. On the other hand, a strong-line approximation to the transmission function was used throughout. A bulk transmission for the 15μ CO_2 band was utilized, without temperature dependence in either the integrated line intensity or Lorentz half-width. As Gierasch and Goody have pointed out, the resulting model is not effective for phenomena involving small length scales, such as radiative heating/cooling near a region of sharp variation in temperature or absorption.

It is precisely the latter phenomena which are of greatest interest in the present study. We are especially concerned with (1) the diurnal history of thermal structure near the soil-atmospheric interface and the extremities of a suspended dust layer, and with (2) the impact of relatively small-scale temperature variation on the outgoing planetary spectral radiance such as would be measured by the Mariner 9 Infrared Interferometer Spectrometer (IRIS). The model described in the present paper is most effective for study of variations in heat exchange and thermal structure in the free-atmospheric layers above the daytime convective boundary layer, and in the near-surface regions when the boundary layer is

stably-stratified. Expansion of the model to account for a time-dependent free-convective boundary layer will be described in a forthcoming article. In the present paper, we report these findings which are expected to be little affected by the inclusion of the convective boundary layer.

2. Simulation Procedure

The atmospheric model adopted is that of a 100% CO_2 atmosphere in local thermodynamic equilibrium (LTE), with plane-parallel stratification and negligible Doppler broadening (Pallmann, 1968; Pallmann and Dannevik, 1972). The lower solid surface is assumed horizontal and of silicate composition. The effect on heat exchange of dust suspended in the lowest scale heights is incorporated by considering the increase of effective radiative path length induced by multiple scattering and the additional direct absorption by the dust particulates themselves.

From dynamical scaling considerations and radiative relaxation time estimates, Gierasch and Goody (1968) have inferred that in the first approximation, temperature change due to advection by the mean wind field may be neglected compared with that due to radiative, molecular-conductive, and turbulent-convective transport. Thus, the atmospheric response to surface temperature variation may be investigated without calculating the large-scale horizontal motion field (Gierasch, 1971).

Details of the coupling between Martian soil and atmospheric temperature variation depend crucially on the structure of the CO_2 absorption bands. Since most of the 15μ -band absorbs strongly even under the reduced surface pressure conditions of Mars ($\sim$ 6 mb), a portion of the coupling will occur through the near-surface layers. Strong-line radiative transfer will approximate a diffusion process in these layers, augmented by the conductive-convective heat transports induced by large temperature gradients. On the other hand, spectral "gappiness" and weak-line transmission, each enhanced by atmospheric tenuity, will permit some long-range exchange of energy from the surface to several scale heights and toward space (Drayson, 1972). This longer-range exchange approximates a Newtonian cooling (Kuo, 1968; Schlichting, 1960).

Several factors serve to complicate the integrated radiative-conductive-convective exchange process. Among these are direct absorption of insolation in the near-IR CO_2 bands, the presence of spectral lines of intermediate intensity, substantial variations in gas-kinetic properties along the radiative path length, and the presence of dust-aerosol in the troposphere. One of the effects of the latter is to increase gaseous absorption, since multiple scattering results in a longer effective radiative path length. In addition, the dust particulates may directly absorb both solar and planetary radiation.

At the soil-atmosphere interface, a discontinuity in physico-optical properties occurs, although on a physical basis we may still expect the resultant net flux of heat to remain continuous across the interface. The net heat flux includes contributions from short- and long-wave radiation and molecular-conductive fluxes in the soil and atmosphere. An additional physical constraint is a tendency toward a matching of temperature determined by molecular conduction in the soil sub-system and the radiative-conductive temperature in the atmospheric layers. This tendency is complementary to the LTE condition.

In devising the simulation procedure, we have incorporated to some extent each of the above mentioned physical processes into a computer model, except for turbulent-convective heat transport. To accommodate the latter, the computer-generated temperature profiles have been submitted to a convective adjustment in the appropriate atmospheric region above the constant flux layer. The depth of this convective region has been determined on the basis of complete adiabatic mixing.

Thermal coupling of the soil and atmosphere may be studied as a boundary-initial-value problem through a forward time integration of the applicable heating rate equation. In our context, this relation takes the form

$$\rho c\frac{\partial T}{\partial t}(x,t) = \frac{\partial}{\partial x}(k\frac{\partial T}{\partial x}) + 2\pi\int_o^\infty \rho\kappa_\nu\Big\{\mu S_\nu(0)\exp(-\int_o^x \rho\kappa_\nu ds\mu^{-1}) +$$

$$G_\nu(t)\exp(-b\int_x^{x_s}\rho\kappa_\nu ds) + \int_o^x B_\nu(\xi,t)\frac{\partial}{\partial\xi}\Big[\exp(-b\int_\xi^x \rho\kappa_\nu ds)\Big]d\xi$$

$$+ \int_x^{x_s} B_\nu(\xi,t)\frac{\partial}{\partial\xi}\Big[\exp(-b\int_x^\xi \rho\kappa_\nu ds)\Big]d\xi - 2B_\nu(x,t)\Big\}d\nu,$$

$$0<x<x_s,\ t>0 \qquad (1a)$$

$$\rho_s c_s\frac{\partial T_s}{\partial t}(x,t) = \frac{\partial}{\partial x}(k_s\frac{\partial T_s}{\partial x}),\ x_s<x<x_d,\ t>0 \qquad (1b)$$

where:

T,ρ,c,k	temperature, density, specific heat, and thermal conductivity in the atmospheric (no subscript) and soil subsystem (subscript "s")
x,ξ	depth, measured from top of atmosphere
x_s	soil-atmosphere interface level
x_d	lowest level considered in soil subsystem
$\arccos(\mu)$	solar zenith angle at time t
κ_ν	mass absorption coefficient at frequency ν
B_ν	specific intensity of blackbody emission
G_ν	upwardly-directed specific intensity at the interface level due to thermal emission or diffuse reflection of solar irradiation
S_ν	spectral solar radiation at the actual Sun-Mars distance
b	diffusivity factor.

The functions T, ρ, κ_ν, and B_ν depend on depth and time, while μ and G_ν depend on time.

Continuity of the total net flux of heat at the interface requires that

$$F_n(x_s-0,t) - F_n(x_s+0,t) = 0. \qquad (2)$$

In terms of the relevant component fluxes, this relation represents an internal boundary condition for the level x_s:

$$2\pi\int_0^\infty\int_0^{x_s-o} B_\nu(\xi,t)\exp\left(-b\int_0^\xi \rho\kappa_\nu ds\right)\rho\kappa_\nu d\xi d\nu - \sigma\varepsilon T_s^4(x_s-0,t) +$$

$$2\pi\int_0^\infty (1-\alpha_s)\mu S_\nu(0)\exp\left(-\int_0^{x_s-o}\rho\kappa_\nu ds\mu^{-1}\right)d\nu - k\frac{\partial T}{\partial x} + k_s\frac{\partial T_s}{\partial x} = 0,$$

$$x = x_s,\ t\geq o. \qquad (3a)$$

Here, σ, ε, and α_s represent the Stefan-Boltzmann constant, IR-emissivity, and surface albedo. Matching of temperature at the interface is expressed as

$$T(x_s-0,t) = T_s(x_s+0,t). \qquad (3b)$$

In (1) and (3a), it is assumed that no phase changes of CO_2 occur.

The upper boundary condition at an elevation of 50 km ($x=0$) is set as vanishing incoming thermal radiation and constant temperature. Finally, the lower boundary condition at $x=x_d$ is that of constant temperature.

A quasi-random model using the band parameters of Prabhakara and Hogan (1965) has been chosen for the transmission functions appearing in (1a) and (3a), and a weak- or strong-line limit is employed, based on the magnitude of radiative path length pertinent to a given spectral and geometric interval. Frequency integration is performed over 62 intervals embracing the 1-6μ and 12-18μ vibration-rotation bands. In those atmospheric strata assumed dust-laden, the gaseous transmission is reduced by a factor $\exp(-\beta_d \Delta x)$, where β_d is an "effective absorption" coefficient due to dust, and Δx is the thickness of the layer. The cumulative fraction of irradiated solar energy flux which is contained in the modeled CO_2 near-IR bands constitutes about 9% of the total insolation. With $\beta_d = 0.1\,\text{km}^{-1}$ and the total depth of the dust layer being 30 km, the model thus produces approximately an additional 9%-attenuation of the vertical solar radiation, which is converted into heat within the dust layer. Gierasch and Goody (1972) utilized a 10%-attenuation under grey absorption.

To accomodate the inhomogeneity of temperature, pressure, and density, the transmission function for an extended path is approximated by a product of transmission functions taken over a number of intervening sub-layers, within each of which the gas-kinetic properties do not vary appreciably. The dependence of line intensity and Lorentz half-width on temperature and effective pressure is included in the calculation of individual layer transmission functions.

The integrals over depth in (1a) and (3a) must be evaluated by numerical quadrature. In view of spectral gappiness in the absorption spectrum and inclusion of molecular thermal conduction in the heating-rate equation, we anticipate a relatively complex structure of the vertical temperature profile in the boundary layer. A 52-point quadrature formula has been adopted, with 7 points distributed in the lowest km, and generally a 1 km spacing in the region between 1 and 50 km. This resolution restricts the relative variation of Planck function to $\lesssim$ 3% in a given layer, under representative conditions. The same spacing is used to construct finite difference approximations to the spatial derivatives in (1a), while a 2-cm increment is used in the soil sub-system.

From the estimates of Goody and Belton (1967), the characteristic time for relaxation of thermal perturbations having scales of the order of several meters is in the range of 10^3 sec for the Martian troposphere. On these physical grounds, we may infer that a computational time increment of similar size is required to adequately resolve in time the propagation of temperature waves in the near-surface region. A 15-minute time step was used for all calculations discussed in this note.

The computational procedure begins with calculation of transmission functions, solar spectral irradiance, and atmospheric spectral emission corresponding to the initial time and temperature distribution. These quantities are then combined to form the total (radiative + conductive) heating/cooling function represented on the right-hand-side of (1a). Flux components in (3a) are then computed, and this relation and (1b) are solved for the soil temperature field for the end of the first timestep. Then, (1a) is solved for the new atmospheric temperature field, using (3b) as the lower boundary condition. The new soil-atmosphere temperature profile is then used as input for the next timestep, and new solar spectral irradiances are calculated for the advanced local time. In this manner,

the procedure continues through the total interval of time desired for the simulation.

Numerical values for physico-optical properties of the simulated soil material were derived through an independent parametric study, in which the JPL (1968) thermal inertia values were adjusted until calculated diurnal surface temperature variation matched that suggested by recent Mariner radiometric scans. Raw spectral solar radiation data are those reported by Robinson (1965), adjusted to the Martian season and latitude relevant to a given simulation.

The initial atmospheric sounding data are derived from preliminary Mariner 9 IRIS inversion profiles kindly furnished by Drs. Hanel and Pearl of the Goddard Space Flight Center, and correspond to 1900 local Martian time (LMT), latitude 38°S, and solar declination -23° (Southern hemisphere summer).

3. Some results and preliminary interpretation

Numerical output of the model for each timestep basically consists of the thermal structure between the levels of 60 cm soil depth and 50 km atmospheric height, radiative fluxes of solar, atmospheric, and surface origin in each of 62 wave number intervals between 1.29 and 18.02μ, and the

radiative and molecular-conductive heating/cooling rates at each computational level. Results presented here are based on two simulations, each representing an interval of 24 Martian hours. The first case, designated "dust-free", utilizes as initial data the Mariner 9 IRIS inversion profile (Hanel et al., 1972) mentioned previously, with a starting time of 1900 LMT. The second case uses an identical initial sounding and starting time, but includes a simulated ground-based dust layer of 30 km thickness; this case will be termed "dust-laden".

Since over the night-time hours the radiative conductive model is thermally dissipative, minor inconsistencies between the arbitrary subsoil and surface temperature and the atmospheric sounding tend to dissappear with time, so that by sunrise, the entire temperature profile is thermally "initialized".

Fig. 1 depicts modeled atmosphenic soundings for 0500 and 1600 LMT for each simulation. With regard to the dust-free case, three basic regimes are evident. The lowest regime, from the surface to about 5 km, includes those atmospheric strata dominated by strong-line, short-path, diffusion-like radiative and convective exchange associated with soil surface temperature variation. The regime between

5 and 31 km is "in communication" with surface temperature variation primarily through weak-line exchange, but also undergoes direct solar heating and weak-line losses to outer space. The regime above 31 km is dominated by the upper boundary conditions, i.e., direct solar heating and emission to outer space, and is affected little by soil surface temperature variation, which lags solar forcing by roughly 4 hours.

Soundings from the dust-laden case exhibit essential differences from those of the dust-free simulation primarily in the middle regime (5-31 km; placement of the top of the simulated dust layer at about the same level as the upper bound of the middle regime for the dust-free case is coincidental). Over the daylight hours, this region approaches an isothermal stratification, in agreement with recent Mariner 9 findings showing a tendency towards this structure in the dust-laden mission phases. The top of the dust layer acts as an "effective radiation surface", similar to its radiative response to the solid soil surface. Diurnal temperature variation at the top of the dust layer is nearly 50% of the amplitude of surface temperature variation. Thus, the upper regime (above $\sim$ 31 km) reacts to this effective radiation table in the same way that the lowest regime acts to surface temperature variation in the dust-free case. In

particular, the radiation table induces a statically unstable stratification at the top of the dust layer in the afternoon hours. The lapse rate of the layer was subsequently adjusted to the adiabatic value to reflect convective mixing.

The Mariner 9 IRIS profile was derived by inverting the IRIS radiance measurements obtained during a dust-laden mission phase, to generate a temperature profile assuming a dust-free atmosphere. This initial temperature profile approximates a smoothed version of the modeled 1600 LMT output for the dust-laden simulation, with decreasing fidelity towards the surface. Further study is required to determine to what extent this result is coincidental or significant.

As indicated on the right-hand-side of Fig. 1, the dust-laden profile at 0500 LMT is warmer than the dust-free in the lowest 800 m, an indication of the insulating effect of the dust blanket keeping surface temperature slightly higher in the nocturnal hours. However, in the bulk of the dust layer, a cooling has occurred by 0500 LMT which is substantially larger than in the dust-free case. This is thought to be attributable to the adopted "grey-body" emission of the dust particles, which results in more photons generated in spectral intervals outside the CO_2 absorption bands.

Atmospheric and subsoil temperature profiles in the layers near the interface are shown in Fig. 2, for the dust-free case. The early-morning atmospheric profiles exhibit diffusionlike heat transport characteristics, due to the dual action of strong-line radiative and molecular-conductive transfer. An "effective radiative-conductive diffusivity" may be estimated by L^2/τ where L and τ are the characteristic length and time scales of the Diffusion" process. This diffusivity is found to be $\sim 2 \times 10^5$ cm^2 sec^{-1}, on the basis of data represented in Fig. 2. This compares well with Gierasch and Goody's (1968) scaling estimate of 10^5 cm^2 sec^{-1}, and is similar in order-of-magnitude to a free-convective eddy diffusivity under mildly-unstable conditions. It also tends to corroborate Goody and Belton's (1967) estimate that the time for relaxation of thermal perturbations by radiation and mild turbulent convection should be comparable for a perturbation length scale of hundreds of meters.

Each of the various heat flux components acting at the soil-atmosphere interface are shown as a function of the time of the day in Fig. 3. The limited computational resolution in the atmospheric surface boundary layer cannot produce temperature gradients steep enough to model realistically the removal of heat from the interface by atmospheric conduction. However, the NET curve in Fig. 3 indicates the energy surplus or deficit available to change the interface

temperature. Short-term oscillations of decreasing amplitude evident in the first two hours of the simulation represent the dissipative smoothing of inconsistencies in the arbitrary initial temperature distribution in the interface and subsoil layers.

The fact that the model does not reproduce the initial flux values after 24 hours can be traced to at least two possible causes. One cause related to limited computational resolution has been discussed in the previous paragraph. A second possible cause is that the initial atmospheric temperature profile may not be representative of the local time and season relevant to the IRIS measurement on which the inverted sounding is based. The preliminary Mariner 9 sounding which we utilize was based on an inversion method which assumes a dust-free atmosphere.

Molecular-conductive heat flux in the soil material is a significant fraction of the net flux available for temperature changes, at all times during the 24 hr simulated period. The conductive flux reaches a maximum about 1.5 hours before local noon, in agreement with measurements under comparable terrestrial physical settings (Sellers, 1965).

Atmospheric counter-radiation varies little over the diurnal cycle. Since the concentration distribution of radiatively-active gases remains constant in the model, any temporal variation in counter-radiation can be traced directly

to variations in the temperature distribution, for the dust-free case. The addition of a simulated dust layer results in an increased counter-radiation for all times of the day, as evidenced in Fig. 3. This phenomenon accounts for a higher minimum morning temperature of 198K for the dust-laden case, as compared with 193K for the dust-free simulation.

Height-time cross-sections of the temperature field between 4 and 18 km of altitude are shown in Fig. 4a, b. Because the pattern between the surface and 4 km is nearly unchanged by the presence of dust, it is not shown here. The region between 4 and 18 km is drastically modified by the dust layer during the daylight hours. This regime responds to direct solar heating and to a lesser extent, to interface-temperature variation. The dust-laden layers above 7 km develop a nearly isothermal stratification in the afternoon hours, in agreement with recent Mariner 9 observations. Detailed interpretation of additional features in Fig. 4 will be presented in the near future.

Acknowledgements. The work reported in this note was partially supported under NASA grant NGR 26-006-042. The cooperation of Drs. Hanel and Pearl of the Goddard Space Flight Center in providing Mariner 9 preliminary data is gratefully acknowledged.

REFERENCES

Drayson, S., 1972: Atmospheric radiative transfer by carbon dioxide. Preprints, Conference on Atmospheric Radiation, Fort Collins, Colo., Amer. Meteor. Soc., 77-79.

Gierasch, P., 1971: Dissipation in atmospheres: The thermal structure of the Martian lower atmosphere with and without viscous dissipation. J. Atmos. Sci., 28, 315-324.

Gierasch, P., and R. Goody, 1967: An approximate calculation of radiative heating and radiative equilibrium in the Martian atmosphere. Planet. Space Sci., 15, 1465-1477.

_____, 1968: A study of the thermal and dynamical structure of the Martian lower atmosphere. Planet. Space Sci., 16, 615-646.

_____, 1972: The effect of dust on the temperature of the Martian atmosphere. J. Atmos. Sci., 29, 400-402.

Goody, R., and M. Belton, 1967: Radiative relaxation times for Mars: a discussion of Martian atmospheric dynamics. Planet. Space Sci., 15, 247-256.

Hanel, R., et alii, 1972: Infrared spectroscopy experiment. JPL Tech. Rept. 32-1550, Pasadena, Calif., 27-33.

Jet Propulsion Laboratory, 1968: Mars scientific model. Vol. 1. JPL Document No. 606-1.

Kuo, H.L., 1968: The thermal interaction between the atmosphere and the earth and propagation of diurnal temperature waves. J. Atmos. Sci., 25, 682-706.

Pallmann, A.J., 1968: Radiative heating and cooling functions for the lower Martian atmosphere under the condition of local thermodynamic equilibrium (LTE). Contractor Rept. NASA CR-1044.

Pallmann, A.J., and W. Dannevik, 1972: Transient variation of Martian ground-atmosphere thermal boundary layer structure. Preprints, Conference on Atmospheric Radiation, Fort Collins, Colo., Amer. Meteor. Soc., 288-291.

Prabhakara, C., and J. Hogan, Jr., 1965: Ozone and carbon dioxide heating in the Martian atmosphere. J. Atmos. Sci., 22, 97-109.

Robinson, N. (ed), 1966: Solar Radiation. Amsterdam, Elsevier Publishing Co., 347 pp.

Schlichting, H., 1968: Boundary Layer Theory. New York, McGraw-Hill Book Co., 747 pp.

FIGURE LEGENDS

Fig. 1a. Modeled vertical temperature profiles at 0500 and 1600 local Martian time (LMT), for the dust-free (solid line) and dust-laden (dashed line) conditions. Also shown is the initial (1900 LMT) profile obtained from inversion (Hanel, et al., 1972) of Mariner 9 IRIS measurements by assuming a dust-free atmosphere.

Fig. 1b. Profiles of the difference $\Delta T = T_c - T_d$ in temperature between the dust-free (subscript:c) and dust-laden (subscript:d) simulations, at 0500 and 1600 LMT.

All results based on following simulation parameters: latitude $\phi = -38^{\circ}$, solar declination $\delta = -23^{\circ}$ (Southern hemisphere summer), surface albedo $\alpha_s = 0.25$, surface infrared emissivity $\varepsilon = 1.0$, soil thermal conductivity $k_s = 2.3 \times 10^5$ erg cm^{-1} sec^{-1} K^{-1} (low-porosity silica), and CO_2-gas thermal conductivity $k = 1.33 \times 10^3$ erg cm^{-1} sec^{-1} K^{-1}.

Fig. 2. Vertical temperature distributions in the sub-soil and lower atmospheric layers for selected hours of the Martian day, from the dust-free simulation. For environmental parameters used, see Fig. 1.

Fig. 3. Diurnal history of the various component heat fluxes at the soil-atmosphere interface. EMIS represents the flux of long-wave radiation emitted by the surface, SCON the molecular-conductive heat flux in the soil material, SOL the absorbed insolation, ACR the absorbed flux of atmospheric counter-radiation, and NET the algebraic sum of all component heat fluxes. Solid lines depict results for dust-free conditions, while the dashed lines (shown for EMIS, SOL, and ACR only) relate to the simulated dust-laden conditions. Influence of CO_2-gas thermal conduction is of lesser significance at the interface, and curve is not shown.

Fig. 4a,b. Height-time cross-sections of the modeled temperature field (deg. K) between 4 and 18 km for (a) dust-free, and (b) dust-laden conditions. Approximate extremal lines are dashed.

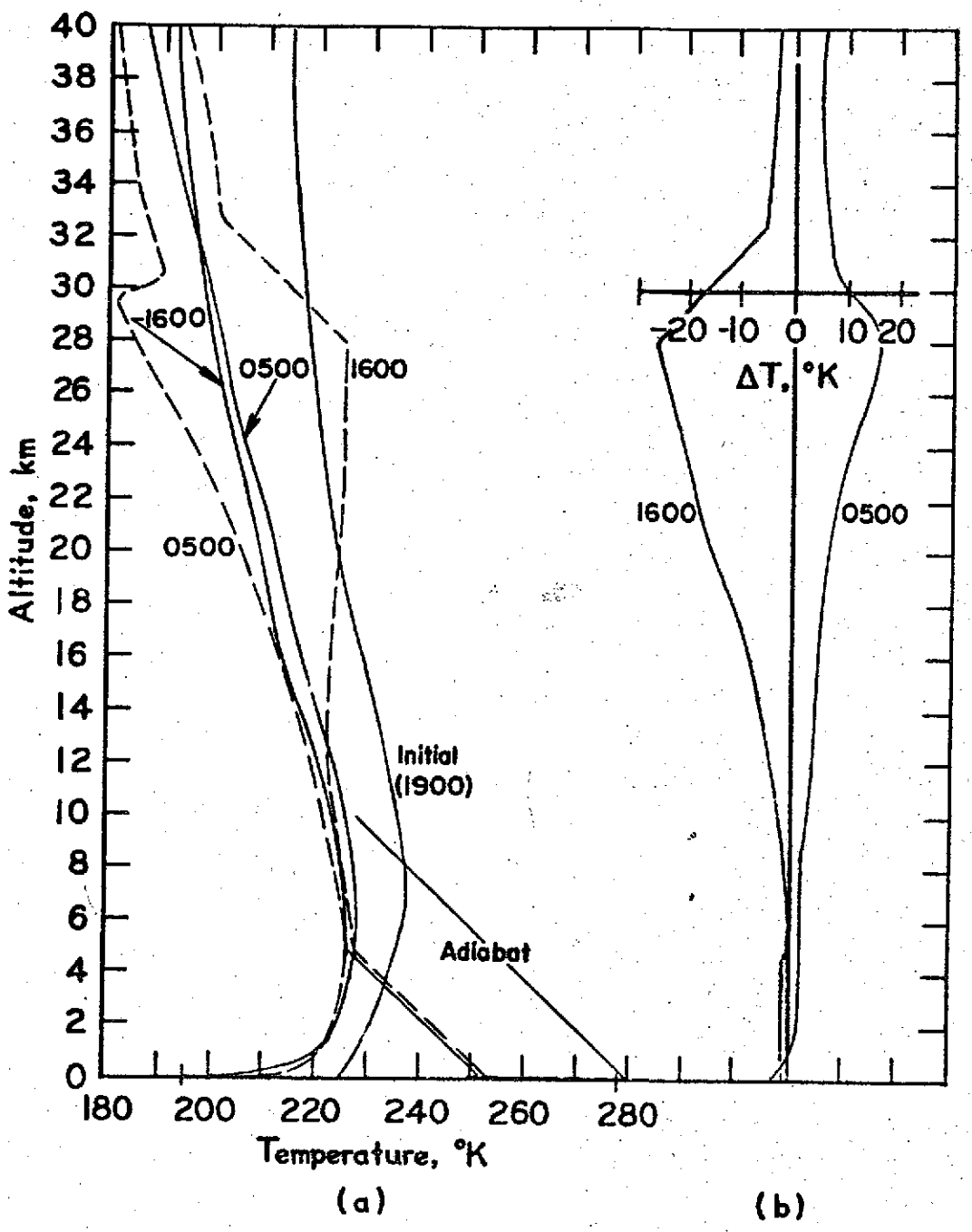
Altitude, km
Temperature, °K
ΔT, °K
1600
0500
1600
0500
0500
1600
Initial
(1900)
Adiabat
(a)
(b)

Fig. 1

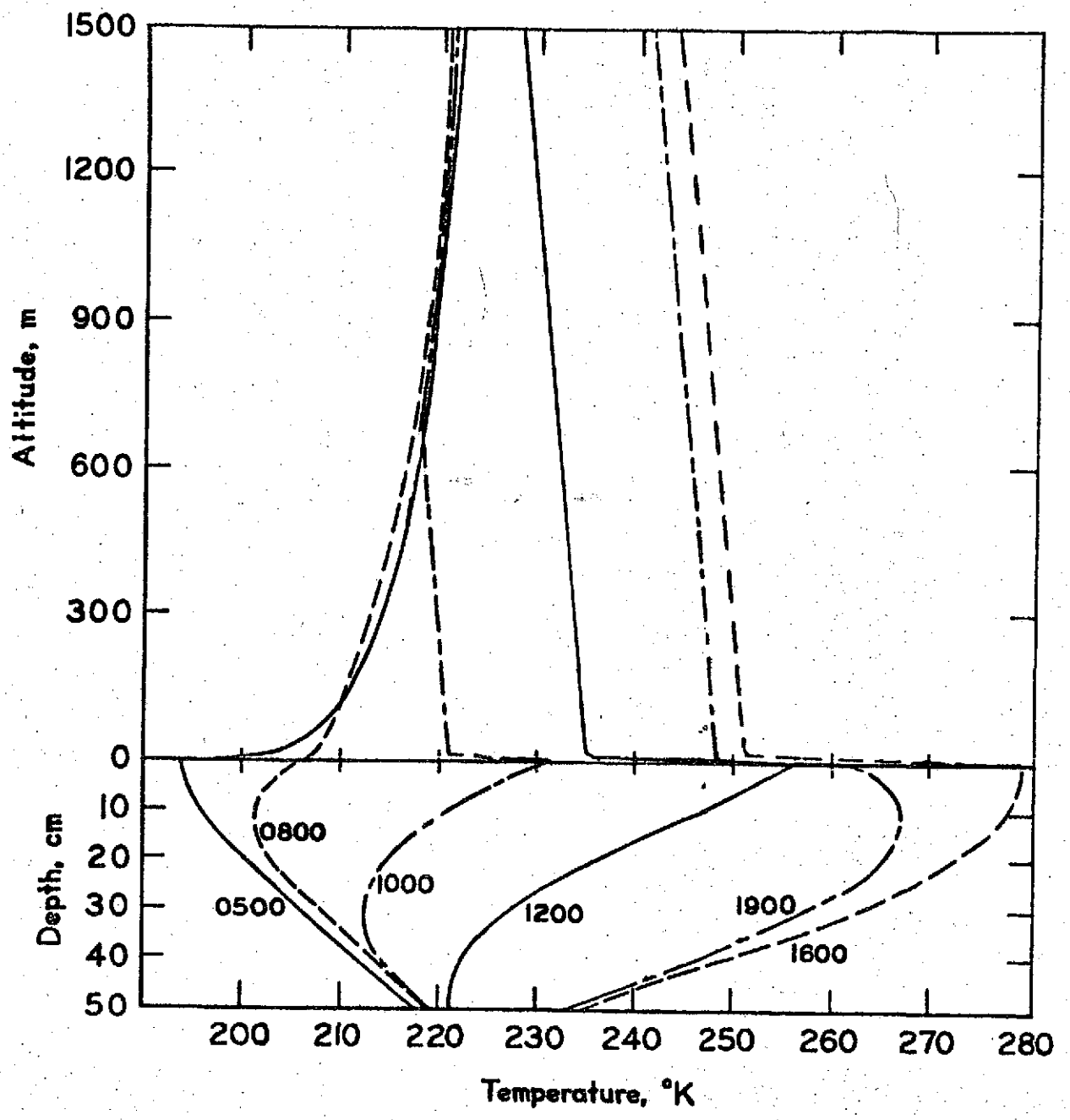
1500
1200
900
600
300
0
Altitude, m
10
20
30
40
50
Depth, cm
0800
1000
0500
1200
1900
1600
200
210
220
230
240
250
260
270
280
Temperature, °K

Fig. 2.

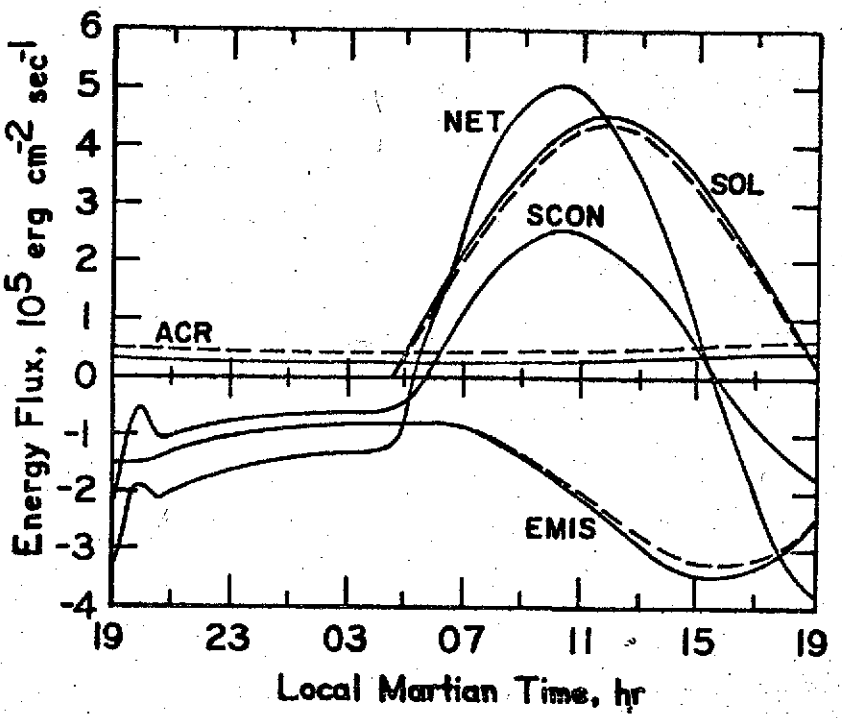
Energy Flux, 10^5 erg cm^{-2} sec^{-1}
6
5
4
3
2
1
0
-1
-2
-3
-4
NET
SOL
SCON
ACR
EMIS
19
23
03
07
11
15
19
Local Martian Time, hr

Fig. 3

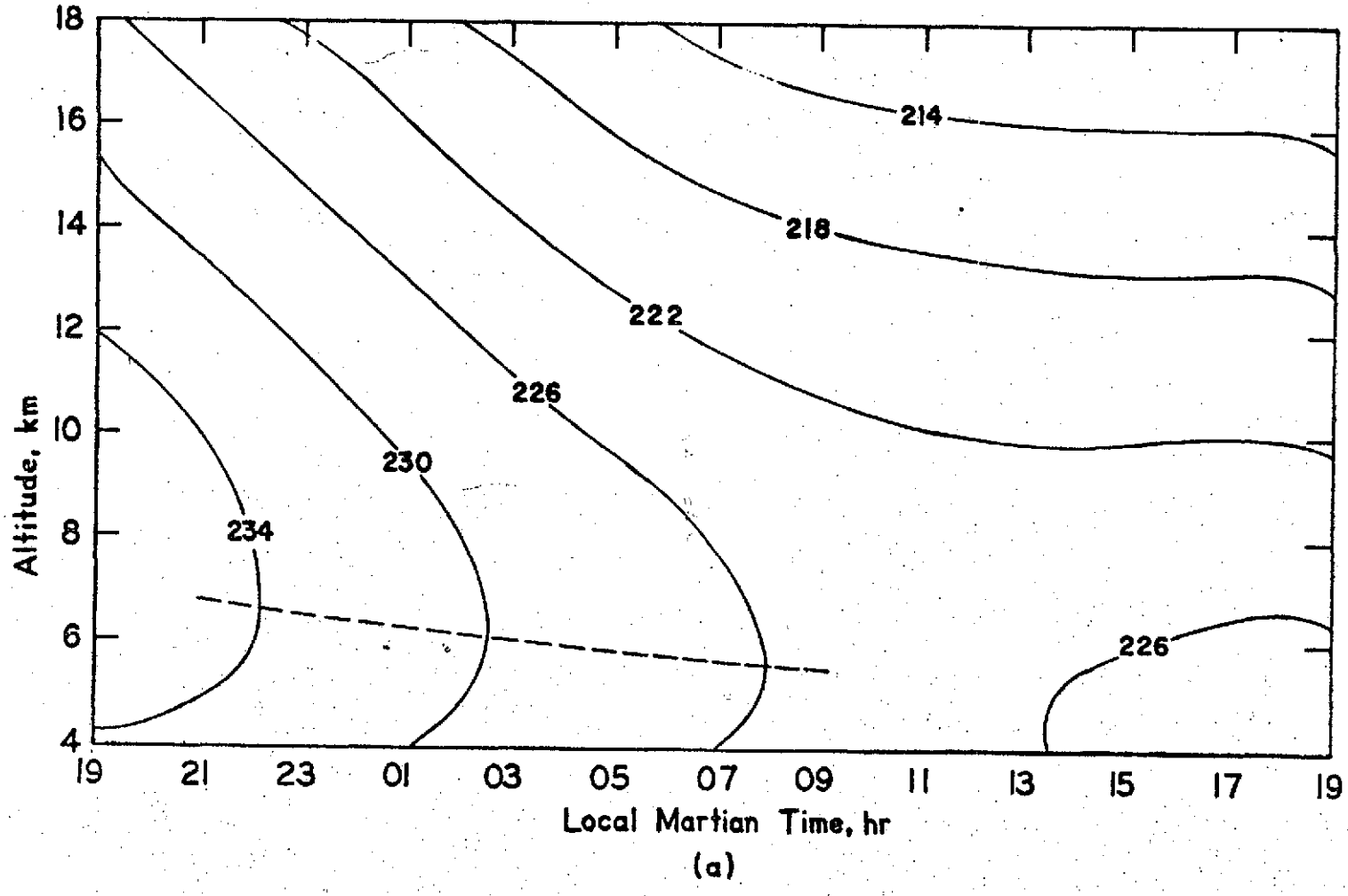
18
16
14
12
10
8
6
4
Altitude, km
214
218
222
226
230
234
226
19
21
23
01
03
05
07
09
11
13
15
17
19
Local Martian Time, hr
(a)

Fig. 4a

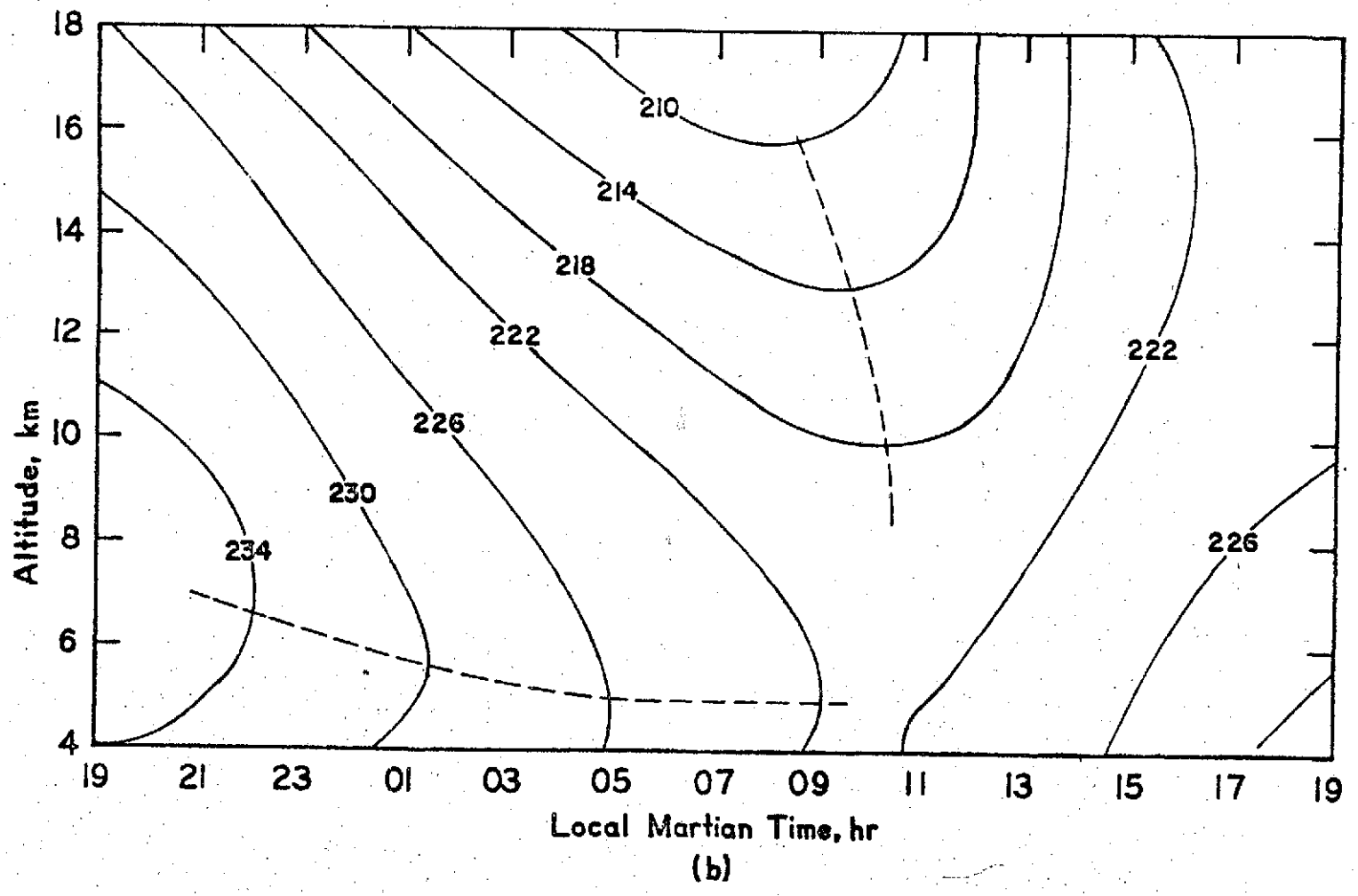
18
16
14
12
10
8
6
4
Altitude, km
210
214
218
222
226
230
234
222
226
19
21
23
01
03
05
07
09
11
13
15
17
19
Local Martian Time, hr
(b)

Fig. 4b